SYNTHESIS AND CHARACTERIZATION OF ZINC AND FERRITE BASED PHOTOCATALYST FOR DYE DEGRADATION IN WATER

By

Engr. Aqsa Javed

Registration No. 00000328084

Supervisor

Dr. Musharib Khan

Institute of Environmental Sciences & Engineering (IESE)

School of Civil & Environmental Engineering (SCEE)

National University of Sciences & Technology (NUST)

Islamabad, Pakistan

2024

SYNTHESIS AND CHARACTERIZATION OF ZINC AND FERRITE BASED PHOTOCATALYST FOR DYE DEGRADATION IN WATER

By

Engr. Aqsa Javed

Registration No. 00000328084

Supervisor

Dr. Musharib Khan

A thesis submitted in partial fulfillment of the requirement for the degree of Master of Science in Environmental Engineering

Institute of Environmental Sciences & Engineering (IESE)

School of Civil & Environmental Engineering (SCEE)

National University of Sciences & Technology (NUST)

Islamabad, Pakistan

2024

Approval Certificate

Certified that the contents and form of the thesis entitled

"Synthesis and characterization of zinc and ferrite based photocatalyst for dye degradation in water"

Submitted by

Ms. Aqsa Javed

Has been found satisfactory for partial fulfillment of the requirements of the degree of Master of Science in Environmental Engineering.

Supervisor: ....

Dr. Musharib Khan

Assistant Professor

SCEE (IESE), NUST

Co-Supervisor: ....

Dr. Fahad Azad

Associate Professor

SNS, NUST

GEC Member: ....

Dr. Rashid Iftikhar

Assistant Professor

SCEE (IESE), NUST

GEC Member: ....

Dr. Waheed Miran

Associate Professor

SCME, NUST

THESIS ACCEPTANCE CERTIFICATE

It is certified that final copy of MS/MPhil Thesis written by Ms. Aqsa Javed (Registration No: 00000328084) of SCEE (IESE) has been vetted by the undersigned, found complete in all respects as per NUST Statues/Regulations, is free of plagiarism, errors, and mistakes, and is accepted as partial fulfilment for the award of MS/MPhil degree. It is further certified that necessary amendments as pointed out by GEC members of the scholar have also been incorporated in the said thesis.

Signature (Supervisor): _____

Dated: 10/10/2024

Signature (Co-supervisor): _____

Dated: 10/10/24

Signature (HoD): _____
Dr. Hassan Anwer
Assistant Professor
HoD Environmental Engineering
SCEE (IESE), NUST
H-12 Islamabad

Dated: 10-10-2024

Signature (Associate Dean): _____
PROF DR MUHAMMAD ARSHAD
Associate Dean SCEE (IESE)
NUST H-12, Islamabad

Dated: 10.10.24

Signature (Principal & Dean SCEE): _____
PROF DR MUHAMMAD IRFAN
Principal & Dean
SCEE, NUST

Dated: 10 OCT 2024

ii

CERTIFICATE OF APPROVAL

This is to certify that the research work presented in this thesis, entitled "Synthesis and Characterization of zinc and ferrite based photocatalyst for dye degradation in water" was conducted by Ms. Aqsa Javed under the supervision of Dr. Musharib Khan.

No part of this thesis has been submitted any where else for any other degree. This thesis is submitted to SCEE (IESE) in partial fulfillment of the requirements for the degree of Master of Science in field of Environmental Engineering, School of Civil and Environmental Engineering, National University of Sciences and Technology, Islamabad.

Student Name: Aqsa Javed   Signature: _____

Guidance and Examination Committee:

    a) Dr. Rashid Iftikhar   Signature: _____
        Assistant Professor
        SCEE (IESE)

    b) Dr. Waheed Miran   Signature: _____
        Associate Professor
        SCME, NUST

Co-Supervisor: Dr. Fahad Azad   Signature: _____
        Associate Professor
        SNS, NUST

Supervisor: Dr. Musharib Khan   Signature: _____

        Assistant Professor

        SCEE (IESE)

HoD: Dr. Hassan Anwer   Signature: _____

Dr. Hassan Anwe
Assistant Professo
HoD Environmental Engineerin
SCEE (IESE), NUS
H-12 Islamaba

Associate Dean: Dr. Muhammad Arshad   Signature: _____

PROF DR MUHAMMAD ARSH
Associate Dean SCEE (IES
NUST H-12, Islamabad

Principal & Dean SCEE: Signature: _____

PROF DR MUHAMMAD IRFAN
Principal & Dean
SCEE, NUST

PLAGIARISM CERTIFICATE

I certified that this research work presented in the thesis titled "**Synthesis and characterization of zinc and ferrite based photocatalyst for dye degradation in water**" is my own work. Thesis has significant new work/knowledge as compared to already published or under consideration to be published elsewhere. No sentence, equation, diagram, table, paragraph or section has been copied verbatim from previous work unless it is placed under quotation marks and duly referenced. This thesis has been checked for plagiarism using Turnitin and found within limits as per HEC plagiarism policy and instructions issued from time to time.

Signature of student _____

Date 10th Oct, 2024 _____

Signature of Supervisor _____

iv

AUTHOR'S DECLARATION CERTIFICATE

I declare that that this research work titled "**Synthesis and characterization of zinc and ferrite based photocatalyst for dye degradation in water**" is my own work. The work has not been presented elsewhere for assessment. The material that has been used from other sources as been properly acknowledged/referred.

Student Signature: _____

Student Name: Ms. Aqsa Javed

Date: 10th Oct, 2024

Dedication

This research is dedicated to my loving, caring, and hardworking parents whose efforts and sacrifice have made my dream of having this degree a reality, words cannot adequately express my deep gratitude to them.

"O My Sustainer, Bestow on my parents your mercy even as they cherished me in my childhood".

Acknowledgements

TABLE OF CONTENTS

List of Abbreviations

AOPs	Advanced Oxidation Process
BOD	Biological Oxygen Demand
BET	Brunner-Emmett-Teller
COD	Chemical Oxygen Demand
CB	Conduction Band
FTIR	Fourier Transform Infrared Spectroscopy
MB	Methylene Blue
TOC	Total Organic Carbon
XRD	X-ray Diffraction
UV	Ultraviolet
VSM	Vibrating Sample Magnetometer
WASH	Water, Sanitation and Hygiene

List of Tables

List of Figures

ABSTRACT

Due to increase in water pollution around the globe due to industrial wastewater, there is an increased focus on photocatalytic degradation for treatment of industrial wastewater. For this study, zinc oxide (ZnO) and zinc ferrite $Zn(Fe_2O_4)$ have been synthesized via co-precipitation route and used as photocatalyst for degradation of methylene blue (MB) under visible light irradiation. The $ZnO-ZnFe_2O_4$ composite is successfully fabricated as photocatalyst and its photocatalytic activity for methylene blue (MB) degradation is successfully analyzed while comparing its efficiency with the induvial material. The characterization of three photocatalyst has been carried out utilizing XRD, FTIR, RAMAN, SEM-EDX, BET and VSM. These techniques confirm the structural, morphological, chemical and magnetic properties of synthesized photocatalysts. The photocatalytic degradation was carried out for all materials while keeping pH, temperature, initial dye concentration and catalyst dosage same. The results showed that ZnO showed highest degradation rate of 98.45% followed by $ZnFe_2O_4$ and $ZnO-ZnFe_2O_4$ composite under irradiation time of 120 minutes. The kinetics results showed that the photocatalytic degradation reaction adheres to pseudo first order reaction. Posts photocatalytic XRD analysis showed the stability of synthesized photocatalyst after degradation process. Mineralization analysis showed that $ZnO-ZnFe_2O_4$ composite showed the highest mineralization of organic contaminants. The study indicates that $ZnO-ZnFe_2O_4$ composite can be used as cost effective photocatalyst with improved recyclability due to its magnetic properties, for degradation of hazardous organic dyes from aqueous solutions.

Keywords: Photocatalysis, Textile wastewater, Dye degradation, Advanced oxidation process, Material synthesis

1 INTRODUCTION

1.1 Background

Water is one of the most critical survival elements on earth. It is among the most important elements required by all living beings on earth in equal measure. Among the many direct uses of water, the most important use is to support life. Although water is available in a plenty amount with 71% of the earth area covered with water body, major portion of it is either in sea or in the form of huge glaciers and ice caps. Whereas the right to clean, safe water is preserved more in international treaties, much of the world's population lack access to clean water. Due to increase in people's population, and busy extended industrialization, the pressure of water consumption has enhanced. However, pollution and overuse of water sources and the general unavailability of fresh water has led to a serious problem all over the world. This has culminated in serious difficulties in water supply, use and utilization (Westall & Brack., 2018).

Among the most significant problems of the modern world, freshwater scarcity is one of major concerns. Approximately 785 million people worldwide, especially in the developing region, lack access to safe water for drinking purposes (Teuntje & Kakes., 2020). This is very dangerous to human health given that disease causing pathogens can be easily contracted through water in areas of regions with limited access to clean water. WASH borne diseases are a major killer, especially children under the age of five; diarrhea, cholera and other waterborne diseases are common. There are also social costs greatly affecting the quality of life in such communities: clean water is not available, which slow down economic growth and perpetuates poverty and inequality. This makes water conservation as well as distribution of water a major global concern (Meehan et al., 2020).

Textile industry is one of the major industries around the globe which is growing rapidly. 70% of Asian countries contribute towards the global textile export all over the world (Cellulose et al., 2021). It is an annually growing market with a growth rate of 8.13% (Zhang et al., 2021). There are different types of dyes which are used in textile industry to create different shade requirements, which results in the production of textile wastewater. Almost 280,000 tons of textile wastewater is generated all over the world annually. 15% of this effluent is being sent directly into the fresh water bodies without any treatment (Neoh et al., 2016). This results in the environmental degradation

and addition of contaminants in water. The textile effluent has high amount of COD, BOD, pH and temperature and when these contaminants interact with sunlight, they disrupt the whole food chain. This has a very negative impact on algal life, marine growth and photosynthetic activity (Holkar et al., 2016). These dyes also have a potential negative impact on human health and environment. Methylene blue (MB) is considered to be one of the most prominent dyes that has been used in textile industry. This dye has potential contribution towards mutagenicity, microbial toxicity, hema-toxicity and reproductive damage (Amin et al., 2014).Different treatment methods and technologies are available for treating textile effluent to minimize the impact of wastewater on humans and the environment. The implementation of these treatment methods depends on the process and chemicals used in textile industry. Different primary, secondary and tertiary treatments are available to treat wastewater. Usually, a combination of different treatment technologies is implemented to obtain the desired treatment level. Physical, biological and advanced oxidation methods are available to treat wastewater effluent. The selection on treatment technology depends on the type of influent and level of treatment required. Advanced Oxidation process is an emerging alternative in wastewater treatment. This treatment method can be effectively used to remove dyes and contaminants from wastewater by ozonation, phenton reactions and photocatalysis (Pratap et al., 2023).

Among many other techniques, synthesis of effective catalyst for degradation of toxic dyes has been found to be a promising strategy for degradation of pollutants. One fine example of such catalyst include Zn based nano composites. Zinc Oxide (ZnO) and Zinc Ferrite ($Zn(Fe_2O_4)$) are one of the promising catalyst for dye degradation. Wide band gap, high surface area and increased photocatalytic activity under sun light makes them a good photocatalyst (Tamiji et al., 2020). In this research, a comprehensive and analytical method is used to provide the effectiveness of both catalyst for degradation of methylene blue. This research can be further used to explore their potential application for dye degradation under varying conditions of pH, temperature and other variable factors.

1.2 Problem Statement

Organic textile dyes like methylene blue cause water pollution and are a major environmental and health issue globally. These dyes are typically released to water system by textile, paper as well as some intending industries hence polluting water

bodies. The general dyes which are released into the water are extremely chemically stable and very difficult to decompose. Physical filtration, coagulation and biological treatment do not seem to be very effective in the removal of such organic pollutants, particularly at extremely low concentrations. Photocatalysis, a process carried out through light activated semiconductor materials, has been identified as a very efficient way of degrading organic pollutants in water.

Zinc oxide (ZnO) possesses good photocatalytic activity and is abundant and inexpensive, which makes it a suitable photocatalyst for the degradation of organic pollutants such as methylene blue (MB). Its efficiency is limited by the fact that when they are exposed to ultraviolet (UV) light, the photogenerated electrons and holes recombine rapidly. However, there is still lack of a comprehensive comparative study of ZnO and $Zn(Fe_2O_4)$ and their nanocomposite structures for practical application. In this work, we investigate zinc ferrite $Zn(Fe_2O_4)$ nanocomposites as a potential solution to overcome these limitations. In order to further analyze the photocatalytic effectiveness of ZnO and $Zn(Fe_2O_4)$ nanocomposites for degrading MB under visible light irradiation, a detailed characterization of their structural, morphological, and optical features will be performed because any intrinsic structural changes will effect the performance of photocatalyst. The goal of this research is to determine which nanomaterial is the best photocatalyst for MB degradation by assessing its performance and understanding the underlying processes. This comparative analysis will aid in the development of effective Zn-based photocatalysts that perform degradation under visible light.

1.3 Objectives

The targeted aims and objectives for this research include:

- Synthesis of ZnO and $Zn(Fe_2O_4)$ by co-precipitation method
- Characterization of structural, morphological and chemical properties of ZnO, $Zn(Fe_2O_4)$, and ZnO/ $Zn(Fe_2O_4)$ composite
- Evaluation and comparison of photocatalytic activities of these materials under visible light
- Analyze the stability of synthesized photocatalyst

1.4 Novelty and Significance

The formation of effective and long-lasting techniques for the breakdown of organic contaminants such as methylene blue is critical as it poses a serious threat to the environment and human health. This research has a wide importance as it will tackle important social and environmental problems associated with the treatment of wastewater from textiles. Firstly, effluents full of contaminants and dyes demonstrate the textile industry's substantial contribution to water contamination, which emphasizes on the urgent need for effective corrective measures. Secondly, this method approach offers a way to mitigate the environmental impact of textile dyeing processes by creating effective photocatalytic materials that can break down pollutants such as methylene blue without imparting the post degradation toxicity. In addition, it is imperative for industries to adhere to strict environmental regulations governing the release of pollutants in order to avoid legal consequences and damage to their market. Materials with photocatalysis enable efficiency in current treatment methods which will further lead to regulatory compliance in longer run.

1.5 SDG Mapping

This research work is aligned with SDG 6 and SDG 12 which focus on provision of clean water and responsible consumption and production in industries.

2 LITERATURE REVIEW

2.1 Overview

Water safety is gradually emerging as a prime issue in today's world because of unsustainable planning of urban development, fast rate of industrialization and uncontrolled utilization of natural water resources (Santhosh et al., 2016). Textile industry has a dyeing division that uses 749 tons of synthetic dyes annually and releases 10% of them as effluent. These effluents are toxic as well as carcinogenic and even fatal effects on the aquatic species (Holkar et al., 2016). Several issues are associated with large amount of textile dyes releases into the natural water bodies. These textile dyes impact the development of aquatic organisms because of the elevated levels of BOD, and COD present in textile effluent (Sharma et al., 2019). The existing treatment methods used for the treatment of textile wastewater cannot effectively degrade the dyes as many of the toxic pollutants in the treated effluent are in the form of non-biodegradable organic dyes such as azo dyes and Rhodamine B. Thus, authors have investigated to introduce new techniques of wastewater treatment in textile industry to ensure that the discarded water has no harm to the environment.

2.2 Textile Industry

Textile industry is one of significant contributor to the global economy. These industries use yarns, fibers, fabrics, and other materials that are used as raw materials to create various derivative products, such as clothing, and thus contribute significantly to the economy. In addition to employing a staggering 35 million people worldwide, this industry accounts for 7% of total global exports, which highlights its immense economic importance to the world. The denim industry, one of the foundations of the economy, is a fabric primarily made of colored cotton threads, usually in a blue shade, which is a very widely used fabric. Although the textile industry, in particular the denim industry, is one of the largest economies in the world, it faces a major environmental challenge as a result of the pollution that is generated during its dyeing process (Al-Buriahi et al., 2022).

2.3 Textile Effluent

The quality and quantity of textile wastewater depends on the production process in textile industry. In general there are washing, dyeing and bleaching processes that are involved in the production of fabric. The washing process involves use of chemicals

which end up being the part of effluent. The chemicals which are used during this process include different types of surfactants, Chelating agents, softening agents, emulsifiers etc. Due to this the effluent has high pH, temperature, COD, BOD and metal content. Hence it is very important to treat effluent before discharging it into environment (Al-Buriahi et al., 2022).

2.3.1 Health and Environmental Impacts

The textile industry contributes world's major environmental problems due to the discharge of wastewater from textile industries into freshwater bodies. These effluents are mixtures of contaminants such as naphthol compounds, sulphur, vat dyes, nitrates, acetic acids, heavy metals such as lead, chromium, arsenic etc (Amin et al., 2014). Dyes used in the textile industry have a significant health risk because they are carcinogenic substances. They can have various harmful health impacts on human body due to their toxicity (Mushtaq et al., 2020). During normal temperature, human body is prone to absorb toxic substances which can be absorbed by skin or through organs. This can affect growth of infants and pose significant health risk to humans due to the accumulation of toxic dyes and heavy metals in the body (Manzoor et al., 2020). Dyes that exist in the environment undergo chemical and biological assimilation which prevents re-oxygenation and tend to trap metal ions in the body that accelerates genotoxicity and micro toxicity (Pratap & Kumar., 2023). The extent of environmental damage to human health caused by textile wastewater is shown in Figure 2.1. Textile wastewater also damages bodies of water and aquatic animals. When dyes start accumulating in natural aquatic systems, they block the penetration of sunlight in water, which disturbs the ability of submerged plants and algae to absorb light, leading to reduced rates of photosynthesis and dissolved oxygen levels in the ecosystem. Methylene blue is a textile dye that has been used across various textile industries and is released into the environment. It is harmful if ingested by humans and animals which can lead to skin, eyes, and respiratory tract infection. During the dying and bleaching process in textile industry, heavy metals are released into the environment and become a part of food chain (Meky et al., 2023) . The high pH and temperature of effluents discharged from the textile industry interrupts the oxygen transfer system and self-purification method in natural water bodies. In addition, this effluent clog soil pores,

21

resulting in loss of soil fertility and a hardened soil texture that prevents root penetration.
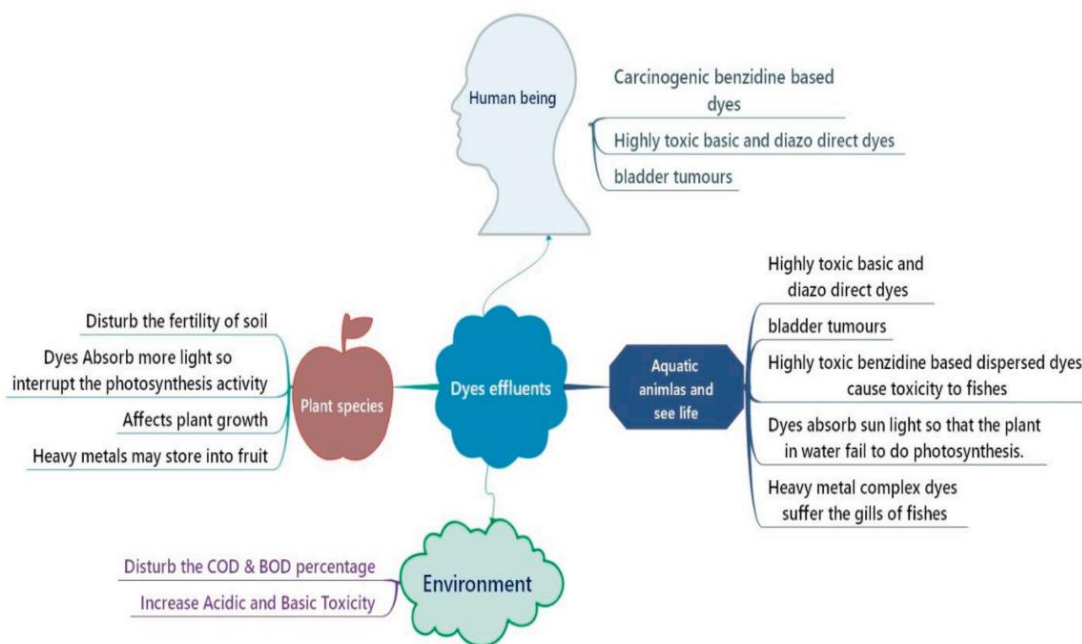
Figure 2.1: Health impacts of textile dye effluent on humans (Pereira & Alves, 2012)

2.4   Treatment Methods

Though dyes which are known to contain mutagens, carcinogens, and allergens have been banned for production and use due to pressure placed on the industry not to release these dangerous compounds into the market but still they are massively used around different industries. Therefore, when treating the textile dye wastewater, just degradation of dye is not enough, its mineralization efficiency improves the remediation process (Pereira & Alves., 2012). Water and wastewater treatment technologies are implemented to reduce the impact of synthesized dyes on environment (Noman et al., 2021). These technologies involve aerobic and anaerobic methods, microbial degradation and pure enzyme and physical separation methods including membrane filtration (micro filtration, nano-filtration, reverse osmosis and electro-dialysis) and sorption techniques. Another advantage of biological treatment is that more organic pollution can be decomposed to achieve complete biodegradation at lower cost in addition to BOD, COD, Solids, dissolved and suspended particles will be eliminated (Noman et al., 2021). Some other treatment methods used in the treatment of textile wastewater include coagulation and flocculation and filtration and other processes. Chemical precipitation, electro-kinetic coagulation and destabilization,

electro-flotation, oxidation reduction is also done. Other than mechanical and chemical methods there are also enzymatic methods used (Pereira & Alves., 2012).

However, the applicability of most of these dyes is less compatible right from its basic applications in routine or standard biological treatments like bio-culturing, bio-typing, and bioremediation which are highly complex (Karthik et al., 2016). Further, the chemical biodegradability of some synthetic textile dye pollutants accompanied with non-biodegradable nature of pollutants due to the stability of the dye remain un degraded in water. It is important to note that most of the available methods used to treat wastewater are ineffective especially for wastewater including synthetic dyes (Noman et al., 2021). The main disadvantage that is sufficient to categorize the physicochemical approaches under the study in terms of their high cost coupled up with low productivity, low flexibility in using the equipment and the outcomes generated to be dealt with (Musa et al., 2021). These physical treatments are efficient in breaking down the dye into smaller particles. These dye molecules are not prone to degradation but contains functional groups, where the bond is not chemically broken down into another substance, and should not be washed down ordinary sewage lines (Pereira & Alves., 2012).In a study, the author implemented a membrane bioreactor to tackle the effluent and recorded a high level of COD reduction at 90% and color removal range at 60-75% (Demirci et al., 2015). In another, study it was noted that the COD removal was observed to increase beyond color degradation when using the activated carbon method together with adsorption. On the other hand, the Fenton's Reagent technique is an effective method that involves the use of chemical reactions to restore the pH. Therefore, the maximum coefficient of the efficiency of water purification in both electrocoagulation methods was the same and 93% removal achieved for COD and for color removal it was 72% (Demirci et al., 2015).

The other emerging technologies that are being applied in novel development are advanced oxidation processes. To a greater extent, the examined AOPs have distinguished themselves in terms of their efficiency in removing pollutants. However, these several techniques cannot be considered cheap and therefore are unattractive. High energy consumption and requirement of reagents are several problems which are associated with them (Pereira & Alves., 2012). Therefore, in relation to the continuation of the promotion of nanotechnologies, the formation of fundamentally new materials and technologies has become an innovative call on the prospective businesses to

produce new, cheap and highly effective wastewater treatment methods that could be applied the idea of which might be reached by means of nanomaterials as catalysts (Cai et al., 2017).

2.4.1.1 Advanced Oxidation Process

Due to several contaminants in waterbodies, global water pollution is a significant issue, causing threats to human, wildlife, and even other living organisms are at high risk. There is an increase in need for designing an efficient, practicable, affordable and sustainable procedure. Advanced oxidation process is one of the most effective methods that can be used to treat textile wastewater and other types of wastewaters due to its benefits including high rate of oxidation and no or less generation of by-products. The advanced oxidation process can be done in several methods like ozone, Fenton, electrochemical, photolysis, sonolysis, and many more. Some of these methods have been used effectively for the degradation of emerging pollutants that cannot be decomposed using conventional methods (Saravanan et al., 2022). This study is confined to the treatment of textile wastewater by advanced oxidation process. Advanced oxidation process may be defined as potential approach for treating wastewater with certain changes and addressing some potential issues.
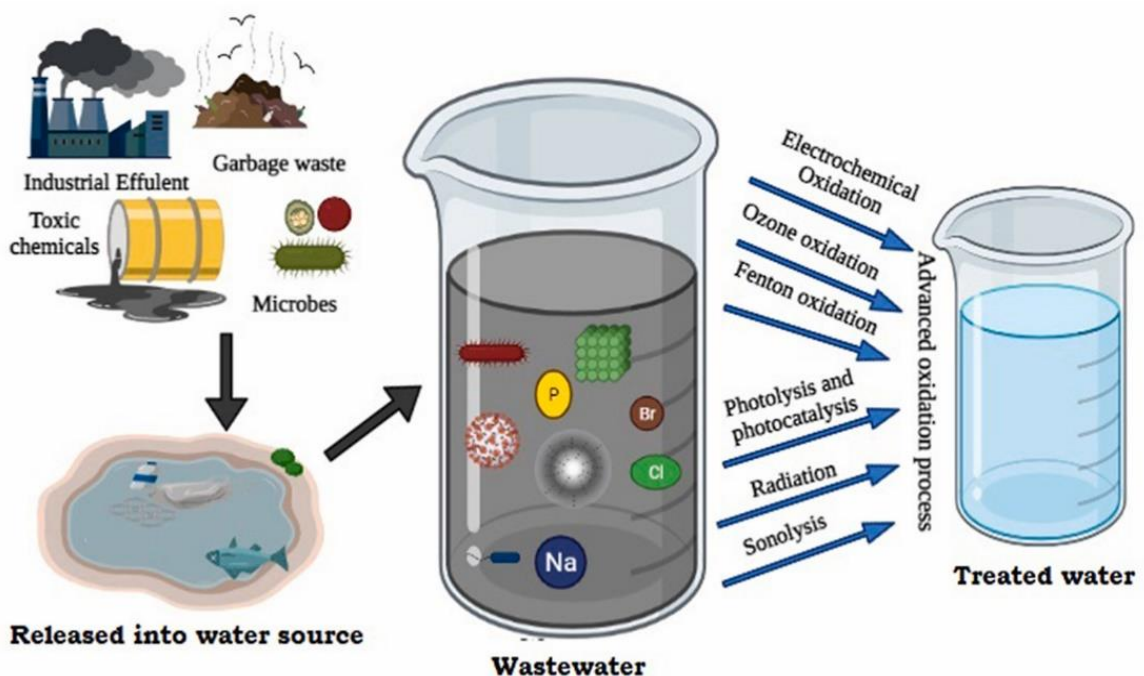
Figure 2.2: Production of industrial effluents and their treatment options (Saravanan et al., 2022)

2.4.1.2 *Photocatalysis*

Photocatalysis is a process in which a photocatalyst, typically a semiconductor material, absorbs light energy and generates electron-hole pairs, which then react with molecules in the environment to produce new chemical species. The potential applications of photocatalysis in various fields have led to extensive research in the development of efficient and stable photocatalysts (Singh et al., 2022). Photocatalysis has numerous applications in various fields, such as water splitting, air purification, and self-cleaning surfaces, due to its ability to generate new chemical species from the reaction of molecules in the environment with electron-hole pairs produced by the photocatalyst. In addition to its applications in environmental remediation, photocatalysis also has potential in the field of energy production. For example, it can be used to convert solar energy into chemical energy, which can be stored and used as a source of fuel. The application of photocatalysis for wastewater degradation has been proven to be highly effective in breaking down organic pollutants and reducing the amount of chemicals needed for the process (Kumari et al., 2023).

Different studies have evaluated and quantified the efficiency of various photocatalysts for textile dye degradation. Research on titanium dioxide (TiO_2), zinc oxide (ZnO), cerium oxide (CeO_2), tin oxide (SnO_2), tungsten oxide (WO_3), and gallium oxide (Ga_2O_3) has shown promising results (Yashni et al., 2021). Among these materials, zinc oxide is one of the most widely used photocatalysts for textile dye degradation. In recent years, there has been a growing interest in using zinc oxide as a photocatalyst for textile dye degradation due to its wide availability and effectiveness in breaking down dye molecules (Yashni et al., 2021). Additionally, studies have investigated the potential applications of zinc oxide and zinc ferrite as photocatalysts. One of the promising applications of zinc ferrite is its potential as a photocatalyst for dye degradation. Zinc ferrite has shown great promise in breaking down organic dyes under visible light, which makes it a highly desirable option for various environmental and industrial applications. Furthermore, the photocatalytic properties of zinc ferrite have been attributed to its unique crystal structure and high surface area, which make it an efficient material for degrading organic pollutants in wastewater and other contaminated environments (Charradi et al., 2022).

2.5 Photocatalytic Degradation of Methylene Blue

The photocatalytic degradation of methylene blue (MB) under solar light using zinc oxide (ZnO) and zinc ferrite $Zn(Fe_2O_4)$ has been explored in various studies. In recent studies, the application of photocatalytic degradation of methylene blue using zinc oxide and zinc ferrite under solar light has been found to be a promising method for the removal of organic pollutants from wastewater. Furthermore, the use of photocatalytic degradation method has the potential to reduce the reliance on chemical treatments for wastewater purification, which can be both costly and harmful to the environment. Zinc Oxide, as a photocatalyst, has demonstrated high efficiency in degrading MB under solar light. Additionally, zinc oxide's photocatalytic properties have been found to be highly effective in breaking down various other pollutants under sunlight, making it a promising material for use in environmental remediation efforts. For instance, ZnO nanoparticles synthesized by chemical co-precipitation showed a remarkable 99% photodegradation efficiency against MB within 90 minutes of solar radiation (Kumar et al., 2019).

Similarly, nano-structured ZnO and Sn-doped ZnO photocatalysts synthesized through microwave heating exhibited enhanced sunlight photocatalytic activity, with Sn-doped ZnO achieving a 13% higher decolorization rate compared to pure ZnO (J. Sun et al., 2011). Furthermore, the increased surface area and reduced electron-hole separation time of the Sn-doped ZnO photocatalysts contributed to their superior photocatalytic performance under sunlight compared to pure ZnO. Additionally, the Sn-doped ZnO photocatalysts demonstrated excellent stability and recyclability, making them promising candidates for practical applications in water treatment and environmental remediation (Sun et al., 2011).On the other hand, the literature does not provide direct evidence of the photocatalytic performance of zinc ferrite $Zn(Fe_2O_4)$ under solar light for the degradation of MB within the provided context. However, the studies on ZnO-based composites, such as the magnetite/zinc oxide (Fe_3O_4/ZnO) nanocomposites, indicate that the incorporation of magnetic components can improve photocatalytic efficiency. Furthermore, researchers have also explored the potential of other metal oxides, such as CuO and Co_3O_4, in combination with ZnO to enhance the photocatalytic performance for various environmental remediation applications (Elshypany et al., 2021). These studies highlight the importance of using composites to achieve efficient and sustainable photocatalytic processes. The $(Fe_3O_4)/ZnO$

nanocomposites synthesized by the solid-state method showed an enhanced photodegradation efficiency of 88.5% for MB degradation under visible light (Elshypany et al., 2021)The results obtained from the Fe_3O_4/ZnO nanocomposites synthesized by the solid-state method demonstrated an enhanced photodegradation efficiency of 88.5% for MB degradation under visible light, which is attributed to the synergistic effect between the two components and their unique structural properties. The findings highlight the potential of this nanocomposite system for efficient organic pollutant degradation under visible light, which could have significant implications for the development of sustainable and environmentally friendly photocatalytic technologies.

In summary, zinc oxide has been proven to be an effective photocatalyst for the degradation of MB under solar light, with modifications such as doping and composite formation further enhancing its photocatalytic performance. While direct evidence for zinc ferrite, studies suggest that ZnO-based composites with magnetic properties, such as $Zn(Fe_2O_4)$/ZnO, can also be effective in solar-driven photocatalytic applications. In addition to the studies mentioned, recent research has also shown promising results for the use of zinc ferrite in various other applications, including water splitting and CO_2 reduction, further highlighting its potential for future use in sustainable energy technologies (Arimi et al., 2018).

2.6 Factors Impacting Photocatalytic Degradation

The process of photodegradation of MB using ZnO and $Zn(Fe_2O_4)$ nanoparticles is a complex multistep process that is influenced by one or more factors. When these nanoparticles are exposed to light, they react to produce electron-hole pairs that reduce and oxidize the adsorbed MB molecules. Aquatic organisms produce specific reactive oxygen species (ROS), such as hydroxyl radicals (•OH), which cause the breakdown of MB into non-hazardous products through oxidation. The efficiency of degradation has been found to be influenced by factors such as catalyst concentration, pH, light intensity, and the initial concentration of MB (Arimi et al., 2018).

The catalytic degradation of methylene blue (MB) organic pollutants, using zinc oxide (ZnO) and zinc ferrite $Zn(Fe_2O_4)$ nanoparticles, results from photoinduced redox reactions on the surface of the catalyst. The generation of electron-hole pairs (e^-/h^+) via photoexcitation is a result of exposing ZnO or $Zn(Fe_2O_4)$ nanoparticles to light energy

equal to or greater than the bandgap energy. ZnO and $Zn(Fe_2O_4)$ possess a wide band gap of 3.17 eV and 2.89 eV, respectively (Davis et al., 2019), which enables them to absorb UV and visible light to initiate photocatalytic processes (Davis et al., 2019).
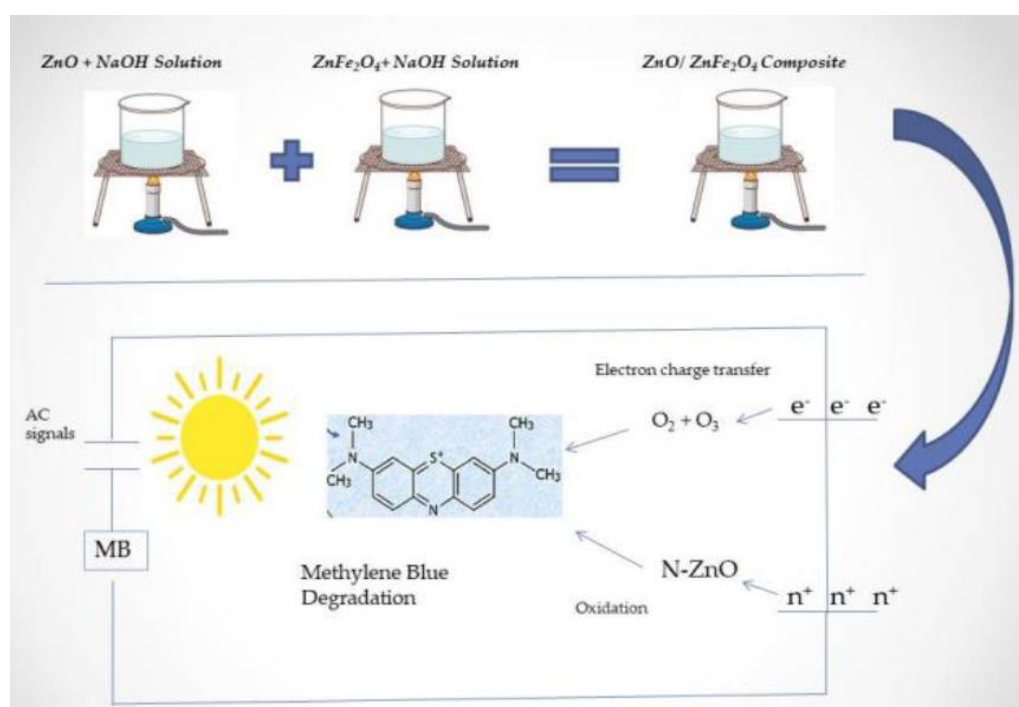
Figure 2.3: Methylene blue degradation under solar irradiation (Davis et al., 2019)

The excitation of photons with energy greater than E_g of ZnO or $Zn(Fe_2O_4)$ results in the transition of electrons from the valence band (VB) to the conduction band (CB), creating electron-hole pairs in the VB. These reactive species can participate in redox reactions. For instance, in the case of organic pollutants such as methylene blue (MB) molecules, the interaction with ZnO or $Zn(Fe_2O_4)$ nanoparticles involves electrostatic interactions, hydrogen bonding, or π–π packing. The presence of MB molecules on the catalyst surface enhances contact between these molecules and the photogenerated electron-hole pairs, thus promoting the degradation reactions (Shandilya et al., 2021). Holes of photogenerated holes (h^+) in the VB of ZnO or $Zn(Fe_2O_4)$ nanoparticles possess a strong oxidation potential (E^o (VB) $\approx$ 2). This energy level, which is approximately 2 eV, enables them to either react with the adsorbed MB molecules or coordinate with water molecules present on the surface of ZnO. As a result, highly reactive hydroxyl radical ($\bullet OH$) molecules are formed. These hydroxyl radicals are potent oxidizing species that can react with and cleave organic structures into less toxic

moieties through mechanisms such as hydroxylation, dealkylation, and ring fission (W. Sun et al., 2018).

2.7 Future Prospect

The future scope of zinc oxide (ZnO) and zinc ferrite $Zn(Fe_2O_4)$ as photocatalysts in advanced oxidation processes (AOPs) appears promising, with ongoing research exploring their efficiency and potential enhancements. In recent years, there has been a growing interest in exploring the potential of zinc oxide and zinc ferrite as photocatalysts in advanced oxidation processes, which could lead to a more sustainable and efficient approach to water treatment and environmental remediation. ZnO has been recognized for its photocatalytic capabilities, particularly in water treatment applications, due to its unique properties and versatility. However, the photocatalytic activity of ZnO can be influenced by the presence of zinc ferrite; studies have shown that increasing the amount of $Zn(Fe_2O_4)$ relative to ZnO can lower the photocatalytic activity (Gegova et al., 2024).Furthermore, it has been demonstrated that the presence of other metal oxides, such as Fe_3O_4, can also affect the photocatalytic performance of ZnO (Gegova et al., 2024). This suggests that the ratio of ZnO to $Zn(Fe_2O_4)$ is a critical parameter for optimizing photocatalytic performance. To achieve optimal photocatalytic performance, it is essential to optimize the ratio of zinc oxide (ZnO) to zinc ferrite $Zn(Fe_2O_4)$ in the photocatalytic system, as this has a significant impact on the overall efficiency of the process. Understanding the relationship between the ratio of ZnO to $Zn(Fe_2O_4)$ and the photocatalytic performance is crucial for developing efficient photocatalytic systems for various applications, such as water splitting and environmental remediation. Further studies are needed to investigate the effects of other parameters, such as light intensity and reaction temperature, on the photocatalytic activity of ZnO and $Zn(Fe_2O_4)$.

Interestingly, the incorporation of other elements, such as iron, into ZnO structures has been shown to extend the photocatalytic activity into the visible light range, which is advantageous for practical applications. Furthermore, the addition of iron into ZnO structures has been shown to enhance the stability and durability of the photocatalytic materials, making them more suitable for real-world applications (Giram et al., 2024).This suggests that the incorporation of other elements into ZnO structures can significantly improve the performance of photocatalytic materials and open up new

opportunities for their use in various industries. Additionally, the formation of heterojunctions, such as Cu_xO/ZnO, has been reported to enhance photocatalytic activity by suppressing electron/hole recombination rates (Villaseñor et al., 2022). These findings indicate that modifications to the ZnO structure, whether through doping or forming heterojunctions, are key areas for future research to improve photocatalytic efficiency. Future research should also explore the potential of other materials, such as metal oxides and nanoparticles, for enhancing the photocatalytic efficiency of ZnO structures.

Furthermore, the applicability of ZnO and zinc ferrite as photocatalysts at an industrial scale is supported by their chemical stability, cost-effectiveness, and high photocatalytic activity under visible light. Zinc ferrite exhibits magnetic properties that facilitate separation in wastewater treatment processes, enhancing its practicality for industrial use (Hedayati et al., 2020). Additionally, the synthesis of ZnO/nickel-zinc ferrite composites has been shown to result in highly efficient photocatalytic activity, with significant degradation rates of organic pollutants such as methylene blue (Hammouche et al., 2021).

However, there are some considerations to be considered. For instance, the photocatalytic activity of ZnO can be influenced by the presence of zinc ferrite; increasing the amount of $Zn(Fe_2O_4)$ with respect to ZnO can lower the photocatalytic activity under UV-light illumination. This suggests that the composition of the photocatalyst is crucial for optimizing performance. Moreover, while ZnO-based photocatalysts have been immobilized on supportive substrates like glass and polymeric materials, further development is needed to address issues such as the lifespan of photogenerated charge carriers and the scalability of these systems.

In summary, ZnO and zinc ferrite have demonstrated potential for industrial-scale photocatalytic applications due to their effective pollutant degradation capabilities and the ease of catalyst recovery. However, the performance is highly dependent on the synthesis methods, composition, and immobilization techniques. Continued research is necessary to overcome challenges related to the efficiency and durability of these photocatalysts in large-scale operations

3 MATERIALS AND METHODS

This chapter outlines the general methodology followed out for carrying out this study. The chapter starts with methodology for material synthesis followed by material characterization, their application for dye degradation and post photocatalytic analysis method.

3.1 Chemicals

The chemicals used for synthesis process include Zinc nitrate Hexahydrate $Zn(NO_3)_2 \cdot 6H_2O$, Ferric Nitrate (Fe $(NO_3)_3$, Sodium Hydroxide (NaOH) and Distilled water (H2O). All these chemicals were purchased from Sigma Aldrich and were used without any further purifications.

3.2 Methodology for Material Synthesis

3.2.1 Synthesis of ZnO

Prepare 1M solution of Zinc nitrate in 300 ml of distilled water. Stir the solution on magnetic stirrer for 15 min to achieve uniform solution. After mixing, heat solution at 90°C at constant stirring. Alongside prepare 2M NaOH solution at 80°C while constant stirring. Drop wise add NaOH solution in $Zn(NO_3)_2$ solution till the pH of solution reaches at 12 and precipitates are formed. Mix the solution at 90°C for 1 hour. Cool the solution at room temperature. Wash the precipitates with distilled water till the pH becomes 7. After washing, centrifuge the solution
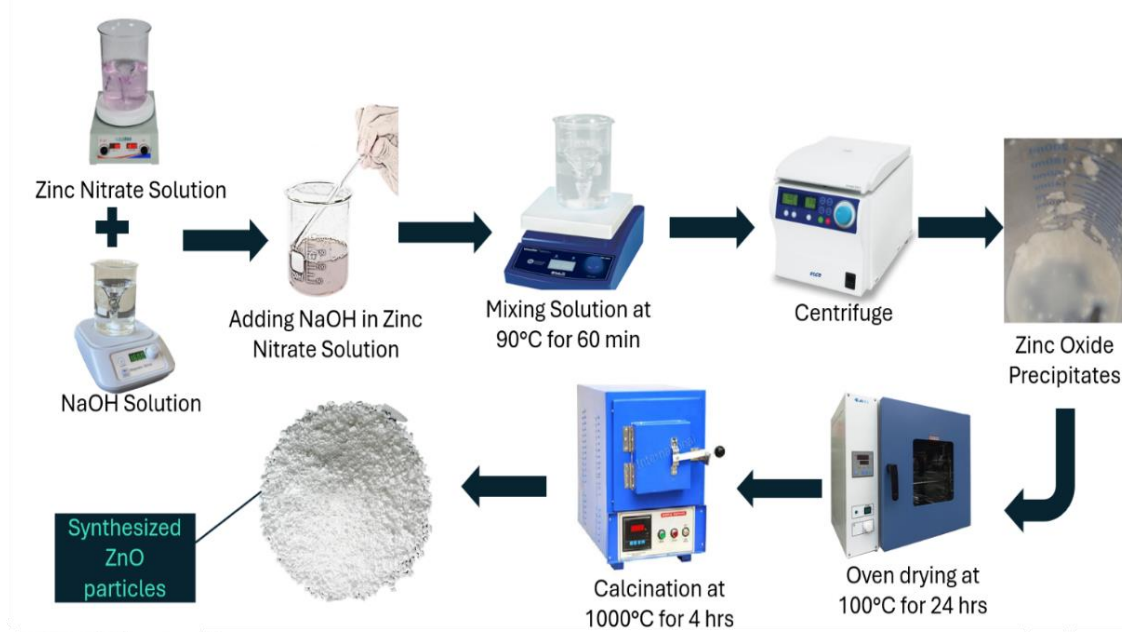
Figure 3.1: Schematic diagram showing synthesis of zinc oxide

and dry it at 100°C for 24 hrs. After drying calculate the ZnO particles in muffle furnace at 1000°C for 4 hrs. White colored ZnO particles are synthesized.

Figure 3.2: Synthesized zinc oxide particles via co-precipitation route

3.2.2 Synthesis of Zn(Fe$_2$O$_4$)

Prepare 0.1M solution of Zn(NO$_3$)$_2$.6H$_2$O and 0.2M of Fe(NO$_3$)$_3$. 9H$_2$O in 300ml of distilled water. After preparation the solutions were continuously stirred for 15 minutes to ensure uniform mixing. Mix both solutions at 90°C for 1 hr. NaOH solution was prepared and added to the solution till the pH ranges to 12 and precipitates are formed.
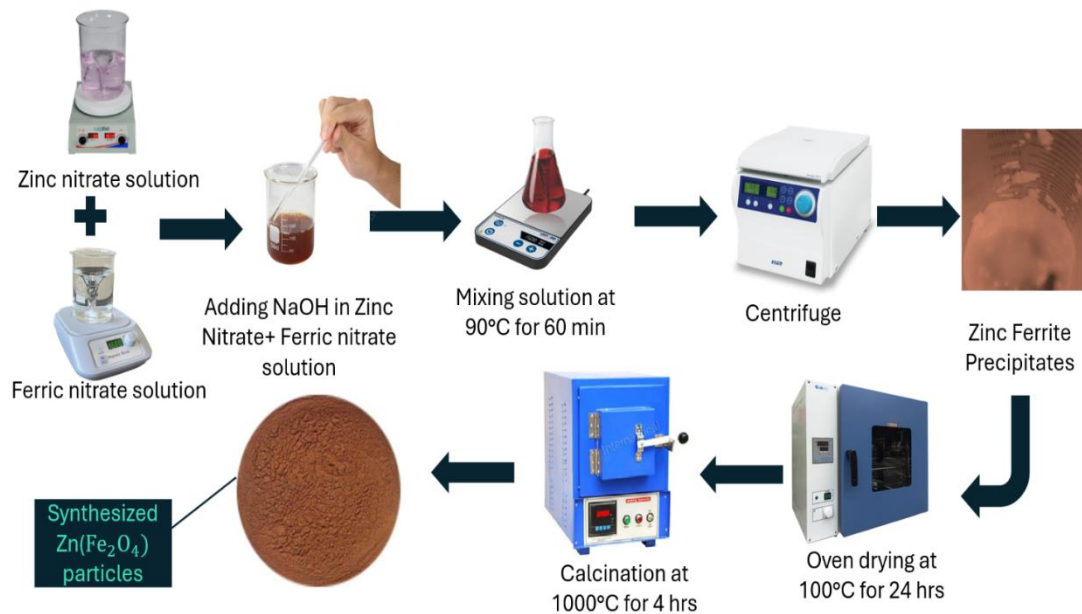
Figure 3.3: Schematic diagram showing synthesis of zinc ferrite

The resulting solution was mixed at 90°C for 1 hour. Cool the solution at Room temperature and wash the precipitates. After washing, centrifuge the solution and dry precipitates at 100°C for 24 hours. The brownish $Zn(Fe_2O_4)$ particles were calcinated in muffle furnace at 1000°C for 4 hrs.

Figure 3.4: Synthesized zinc ferrite particles via coprecipitation route

3.2.3   Synthesis of ZnO/Zn(Fe$_2$O$_4$) Composite

The composite was synthesized by using sonication and stirring method. ZnO and $Zn(Fe_2O_4)$ are dissolved in 50ml of distilled water. ZnO is mixed on magnetic stirrer while $Zn(Fe_2O_4)$ is stirred on sonicator. Both solutions are mixed and dried at 100°C to obtain composite material.
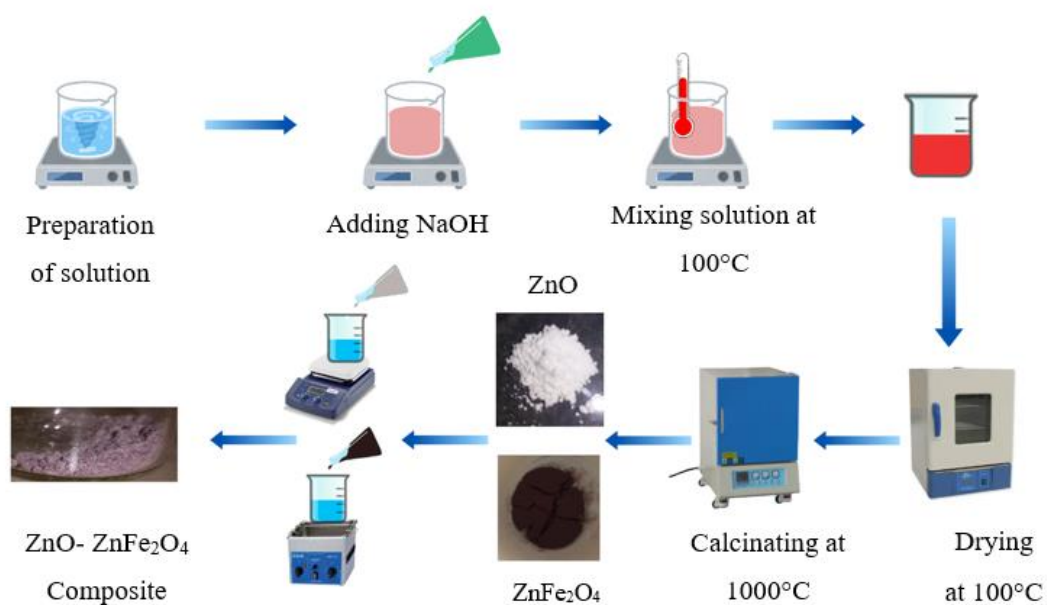
Figure 3.5: Methodology followed for preparation of composite

3.3 Characterization Technique

The structural characterizations of synthesized particles formed was performed using XRD (BRUKER, 2D phaser, XRD Spectrometer) at a wavelength of 0.154 nm of Cu--Kα radiation (40 mA, 40 KV). The analysis was performed using powdered form nanocomposites. The structural components of the sample were investigated in the range of 2θ from 20° to 80°. To further analyze the functional group present in the material, Fourier Transform Infrared Spectroscopy (FTIR) was performed using (PerkinEimer, Spectrum 100, FTIR spectrophotometer). The structural and surface morphology of materials was analyzed by (JSM6940LA, Analytical Low Vacuum, SEM). The elemental composition of materials was observed by energy dispersive X-ray spectroscopy (EDX) (JSM-6490, JEOL, Japan). Brunauer-Emmett Teller (BET) was used to analyze the surface area, pore size and pore volume of synthesized particles. The magnetic properties of materials were examined by Vibrating Sample Magnetometer (VSM) analysis. Raman Spectroscopy was performed to analyze the local structure of materials by scattering light, which provides information about molecular vibrations and crystallinity.

3.4 Preparation of Standard Solutions

Standard stock solution of 1000 ppm was prepared for methylene blue. In order to carry out degradation experiment, it is necessary to have a calibration curve for the dye. For this purpose, 5 solutions of 2ppm, 4ppm, 6ppm, 8ppm, and 10ppm were prepared from the stock solution. Following equation was used to prepare solutions of different concentrations:

$$M_1V_1 = M_2V_2$$

Where M_1 and V_1 are molarity and volume for stock solution where as M_2 is molarity for solution required and V_2 is calculated for each different concentration.

Figure 3.6: Preparation of methylene blue solutions for standard calibration curve

3.5 Evaluation of Photocatalytic Degradation

The photocatalytic performance of all three synthesized particles was carried out in a photocatalytic chamber under visible light. 2ppm of methylene blue solution was prepared to carryout the degradation process. 40 mg of each catalyst was used in 100ml of solution under 36W visible light source. The temperature of solution was maintained at 39℃ $\pm$5 and pH of solution was maintained at 8. The solutions were continuously stirred on a magnetic stirrer at 400rpm for about 120 min.
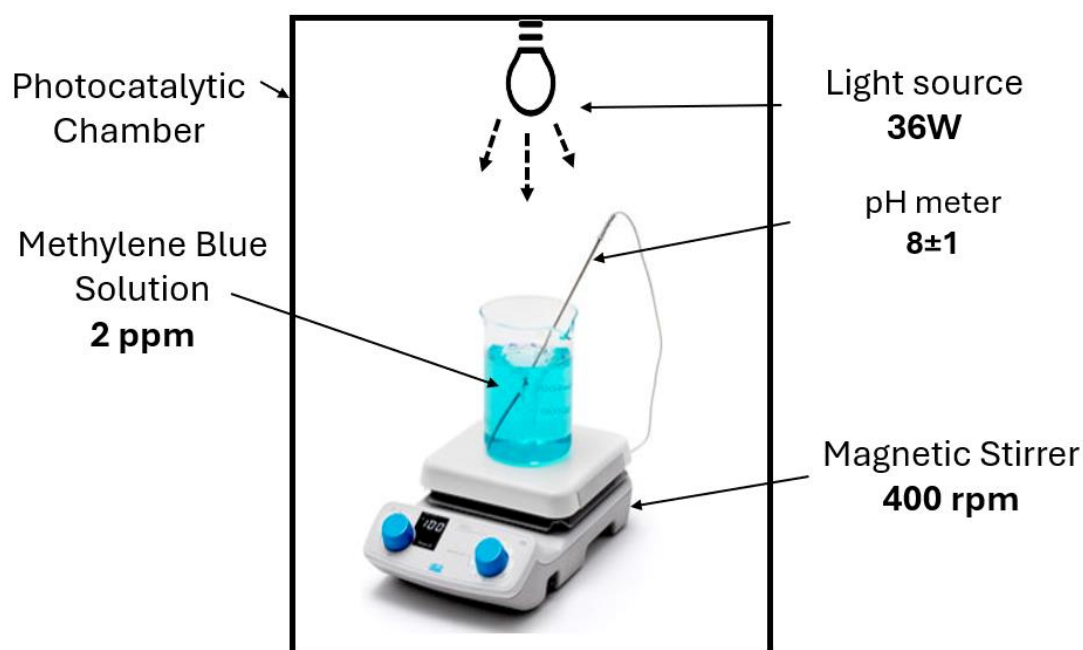
Figure 3.7: Experimental setup for photocatalytic degradation of methylene blue

The formula used to calculate degradation rate is as follow:

$$\% \text{ Degradation} = \frac{C_o - C_t}{C_o} \times 100$$

Where C_o is concentration of dye before degradation and C_t is concentration of dye after degradation at time interval t.

3.5.1 Conditions for Degradation Analysis

Three controlled experiments were performed to analyze the degradation of each material.

i. Degradation of 2ppm methylene blue solution without catalyst under dark condition

ii. Degradation of 2ppm methylene blue solution with catalyst under dark condition

iii. Degradation of 2ppm methylene blue solution with catalyst under light condition

3.6 Phytotoxicity Analysis

After carrying out the degradation experiment, phytotoxicity analysis was performed using degraded product. Mung beans and coco peat was used for carrying it out. 10 mung beans were planted in five pots, and they were fed with normal water, degraded water and polluted water for period of two weeks. After two weeks, shoot length, root length and germination of seeds in each pot was observed.

Figure 3.8: Setup showing mung beans in coco peat

3.7 Post Photocatalytic Degradation Analysis

After photocatalytic degradation, the solution was centrifuged at 4000 rpm using centrifugal machine. This allows to separate the catalyst and degraded solution. Afterwards, XRD and FTIR analysis for catalyst after degradation was carried out to analyze the stability of materials. Total organic carbon (TOC) analysis was carried out for degraded product to study the mineralization of pollutants.

Figure 3.9: Diagram showing post-photocatalytic degradation analysis
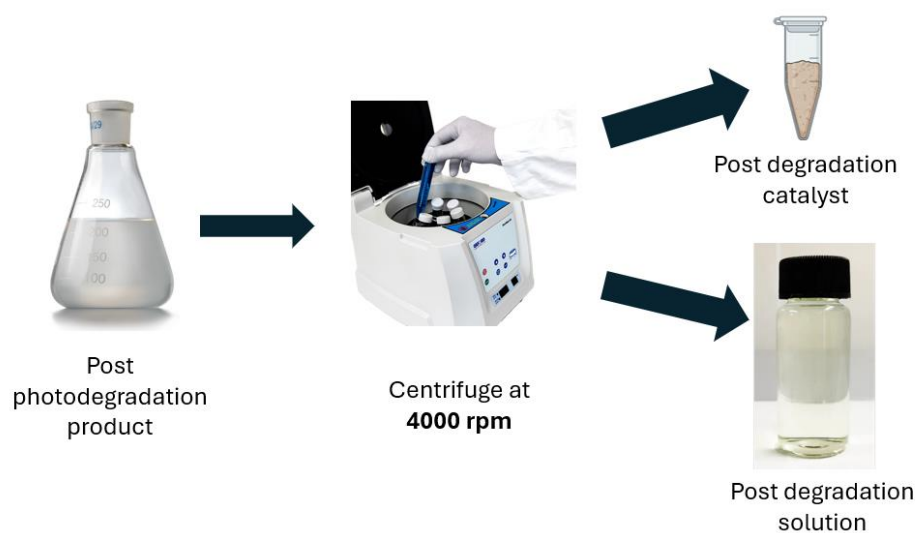
4 RESULTS AND DISCUSSIONS

This chapter outlines the results and provide detailed discussion from the experimentation. It includes the characterization analysis of synthesized materials following with the performance of materials for MB degradation. The chapter ends with comparative analysis for their efficiencies and post degradation analysis after degradation.

4.1 Characterization Analysis

In order to understand the structural, morphological, and chemical characteristics of ZnO and $Zn(Fe_2O_4)$ nanoparticles, characterization analysis is necessary. Scanning electron microscopy (SEM) offers insights into the size and shape of particles, while X-ray diffraction (XRD) gives information on crystal structure and phase purity. By identifying functional groups and surface changes, Fourier-transform infrared spectroscopy (FTIR) advances our understanding of the characteristics of nanomaterials. The specific surface area of solid materials may be calculated using the Brunauer-Emmett-Teller (BET) theory by using gas adsorption data. The energy dispersive X-ray spectroscopy (EDS, also shortened to EDX or XEDS) allows to study chemical and elemental examination of many materials. Raman spectroscopy is a non-destructive chemical analysis technique that offers extensive information on chemical structure, phase and polymorphism, crystallinity, and molecular interactions. VSM is used to study the magnetic behavior of materials by measuring their magnetic moment as a function of an applied magnetic field. It provides information such as hysteresis curves, saturation magnetization, coercivity, and magnetic induction.

4.1.1 XRD Analysis

4.1.1.1 *ZnO*

The figure below shows the XRD pattern of ZnO particles. The data obtained is in accordance with the JCPDS PDF # 36-1451 and the structure is indexed as Hexagonal zincite. The strong diffraction peaks confirm the crystalline nature of ZnO particles. The XRD patterns shows the hexagonal wurzite phase of ZnO particles with a space group $P6_3mc$ (186) (Meky et al., 2023). The peak with 100% intensity is found to be at $2\theta=31.8°$ with *hkl* value of 101. The second highest peak is found at 36.30° with hkl value of 100. Third highest peak is found at 34.46° with *hkl* value of 002. Some
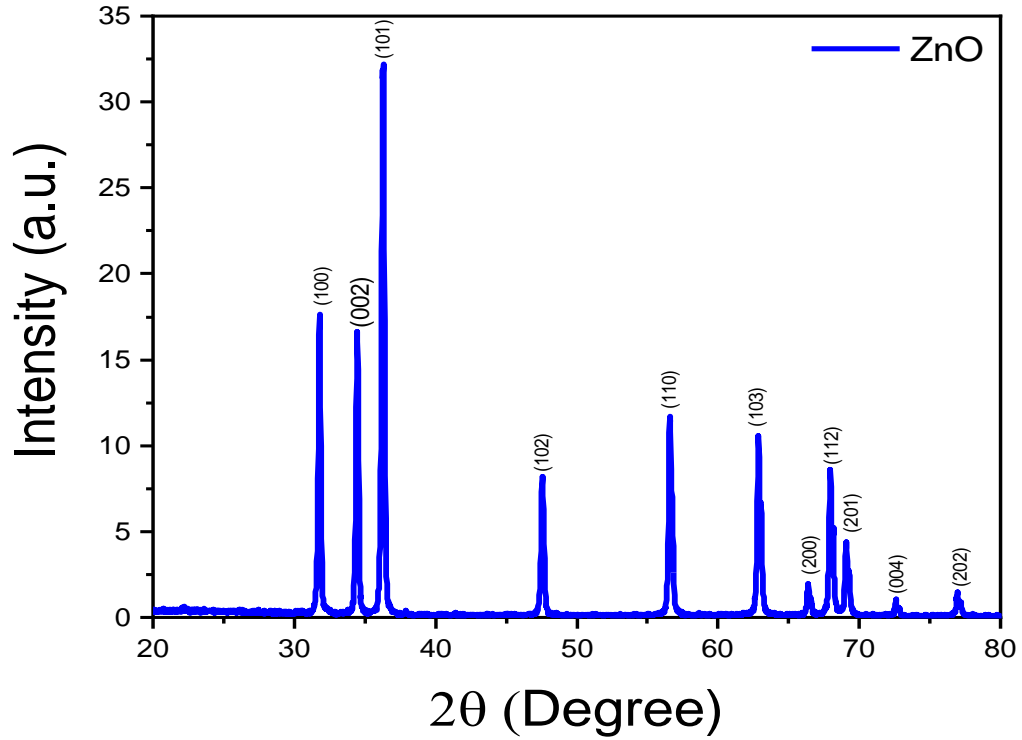
Figure 4.1: XRD pattern for zinc oxide

other peaks are also found due to scattered radiation. No other peaks are detected which shows any kind of impurity (Meky et al., 2023).

4.1.1.2 Zn(Fe$_2$O$_4$)

XRD was used to identify the structures of zinc ferrite. Zinc ferrite has a cubic structure with a space group Fd^{3}m (227) and the parameters found matched well with the JCPDS PDF # 22-1012. According to XRD pattern, peaks at $2\theta= 35.2°$ at 311 plane is the highest peak that confirms the crystalline structure of Zn(Fe$_2$O$_4$) particles. Other peaks at $2\theta= 29.9°$, $36.8°$, $42.8°$, $53.06°$, $56.57°$, $62.2°$ and $73.43°$ at hkl values of 220, 222, 400, 422, 511, 440 and 533 respectively further confirms the cubical phase of spinel zinc ferrite nano composites (Silambarasu et al., 2017).
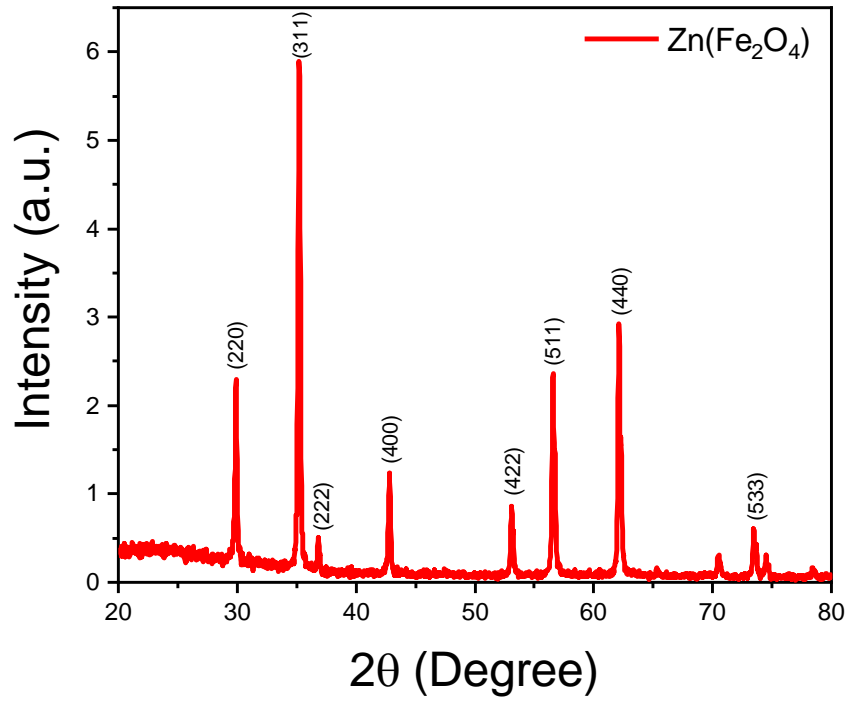
Figure 4.2: XRD pattern for zinc ferrite

4.1.1.3 ZnO-Zn(Fe₂O₄) Composite

The XRD analysis of composite material shows the successful incorporation of ZnO and $Zn(Fe_2O_4)$ nanoparticles. No major peak shift is detected in the XRD pattern. The spinel peaks confirm the formation of crystalline material. The peaks formed at 2θ=
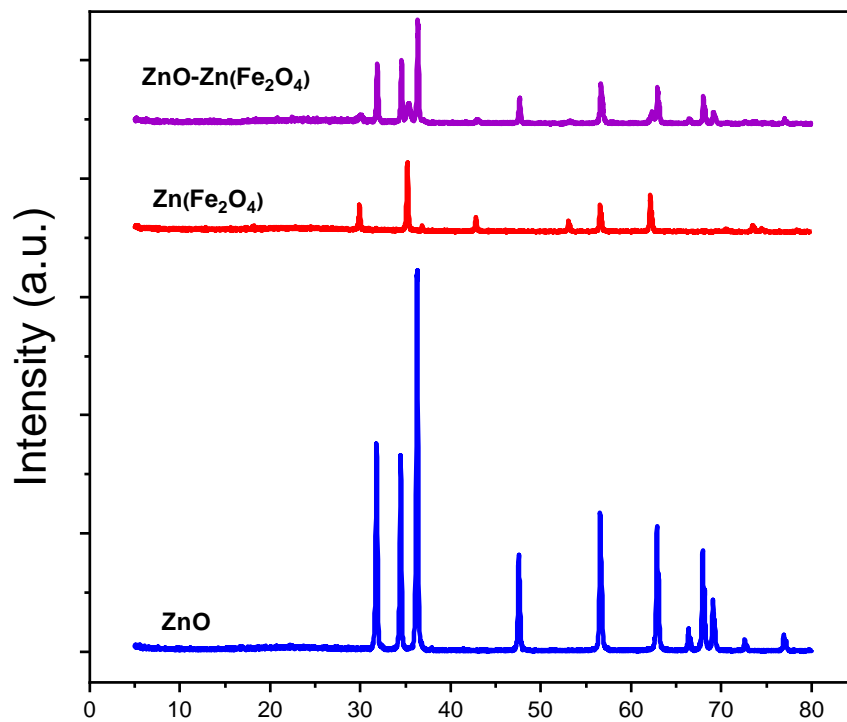
Figure 4.3: XRD pattern for composite

31.8°, 34.5°, 36.34° and 47.6° confirms the presence of ZnO while peaks at 2θ= 56°,62.3° and 62.9° shows the presence of $Zn(Fe_2O_4)$ (Gupta et al., 2019).

4.1.1.4 Williamson Hall Plots

The broadening of diffraction peaks reveals the existence of crystal imperfections, which is identified via XRD peak profile analysis. Crystallite size and lattice strain are the two most important parameters which influence the diffraction peak broadening. The Scherrer formula is commonly used to characterize the impact of crystallite size on XRD peak broadening. However, its main drawback is that it does not account for the lattice's microstructure. Several methods are used to examine microstructural properties including Williamson Hall method. The W-H technique is particularly successful at accurately measuring crystal size and lattice strain. In 1953, G.K. Williamson and his student W.H. Hall introduced a technique that considers the broadening effects of crystallite size (βsize) and strain (βstrain). The broadening effect in diffraction peaks is depending on two factors:

$$\beta_{total} = \beta_{inst} + \beta_{sample}$$

$$\beta_{sample} = \beta_{Crystallite\ size} + \beta_{microstrain}$$

$$= \frac{k\lambda}{D\cos\theta} + 4\varepsilon\tan\theta$$

$$= \frac{k\lambda}{D\cos\theta} + 4\varepsilon\frac{\sin\theta}{\cos\theta}$$

Multiply cos*θ* on both sides,

$$\beta_{total}(\cos\theta) = \varepsilon(4\sin\theta) + \frac{k\lambda}{D}$$

Which makes the straight line equation y = m(x) + c.

41

Table 4.1: Crystallite size of three materials by Williamson Hall method

|	K	λ	FWHM (°)	FWHM (rad)	2θ	θ	θ(rad)	cos θ	D = kλ/Bcosθ
Zinc Oxide	0.9	0.15	0.22	0.004	31.79	15.89	0.26	0.97	37.49
	0.9	0.15	0.21	0.004	34.46	17.23	0.28	0.96	39.06
	0.9	0.15	0.23	0.004	36.28	18.14	0.30	0.96	36.40
	0.9	0.15	0.25	0.004	47.58	23.79	0.39	0.92	34.41
	0.9	0.15	0.29	0.005	56.63	28.31	0.47	0.89	31.08
	0.9	0.15	0.32	0.006	62.91	31.45	0.52	0.87	28.75
	0.9	0.15	0.29	0.005	66.41	33.21	0.55	0.85	31.70
	0.9	0.15	0.34	0.006	67.99	34.00	0.56	0.85	27.45
	0.9	0.15	0.34	0.006	69.13	34.56	0.57	0.84	27.56
	0.9	0.15	0.18	0.003	72.60	36.30	0.60	0.83	53.63
	0.9	0.15	0.32	0.006	77.00	38.50	0.63	0.81	31.04
Zinc Ferrite	0.9	0.15	0.23	0.004	29.90	14.95	0.25	0.97	35.58
	0.9	0.15	0.23	0.004	35.22	17.61	0.29	0.96	36.49
	0.9	0.15	0.15	0.003	36.84	18.42	0.30	0.95	54.02
	0.9	0.15	0.22	0.004	42.81	21.41	0.35	0.94	39.08
	0.9	0.15	0.27	0.005	56.61	28.30	0.47	0.89	32.58
	0.9	0.15	0.28	0.005	62.16	31.08	0.51	0.87	32.34
	0.9	0.15	0.25	0.004	73.50	36.75	0.60	0.82	38.60
	0.9	0.15	0.23	0.004	31.87	15.93	0.26	0.97	36.25
Composite	0.9	0.15	0.22	0.004	34.56	17.28	0.28	0.96	38.26
	0.9	0.15	0.23	0.004	36.36	18.18	0.30	0.96	35.85
	0.9	0.15	0.48	0.008	35.37	17.69	0.29	0.96	17.16
	0.9	0.15	0.25	0.004	47.65	23.83	0.39	0.92	35.04
	0.9	0.15	0.33	0.006	56.71	28.36	0.47	0.89	26.75
	0.9	0.15	0.33	0.006	62.98	31.49	0.52	0.87	27.51
	0.9	0.15	0.34	0.006	68.06	34.03	0.56	0.85	28.00
	0.9	0.15	0.38	0.007	69.14	34.57	0.57	0.84	25.12
	0.9	0.15	51.41	0.897	69.14	34.57	0.57	0.84	0.18
	0.9	0.15	0.47	0.008	62.34	31.17	0.51	0.87	19.53
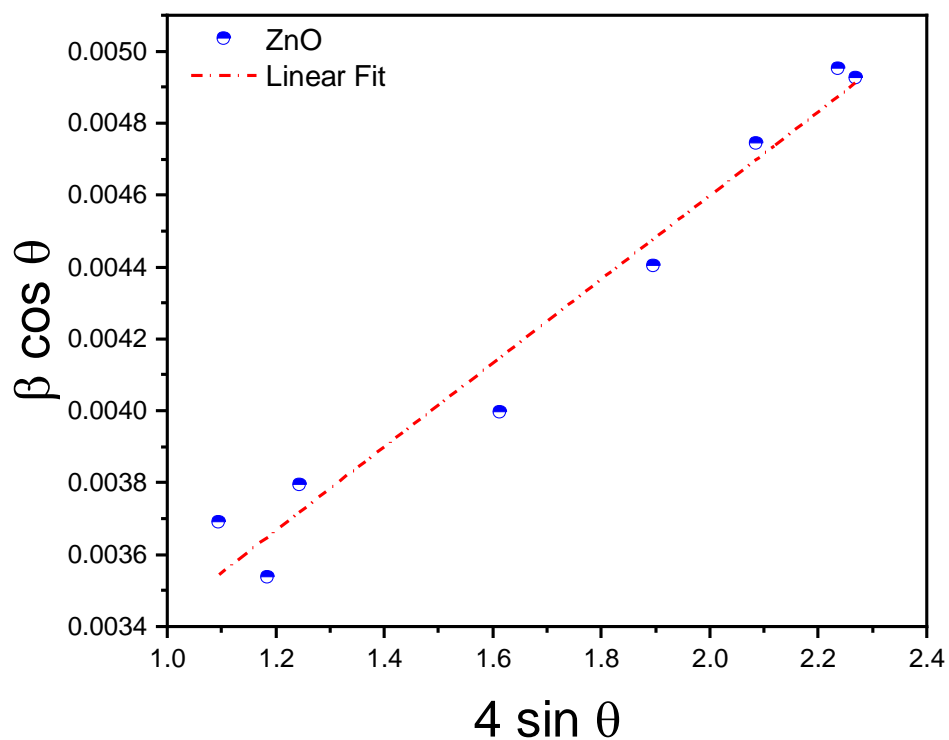
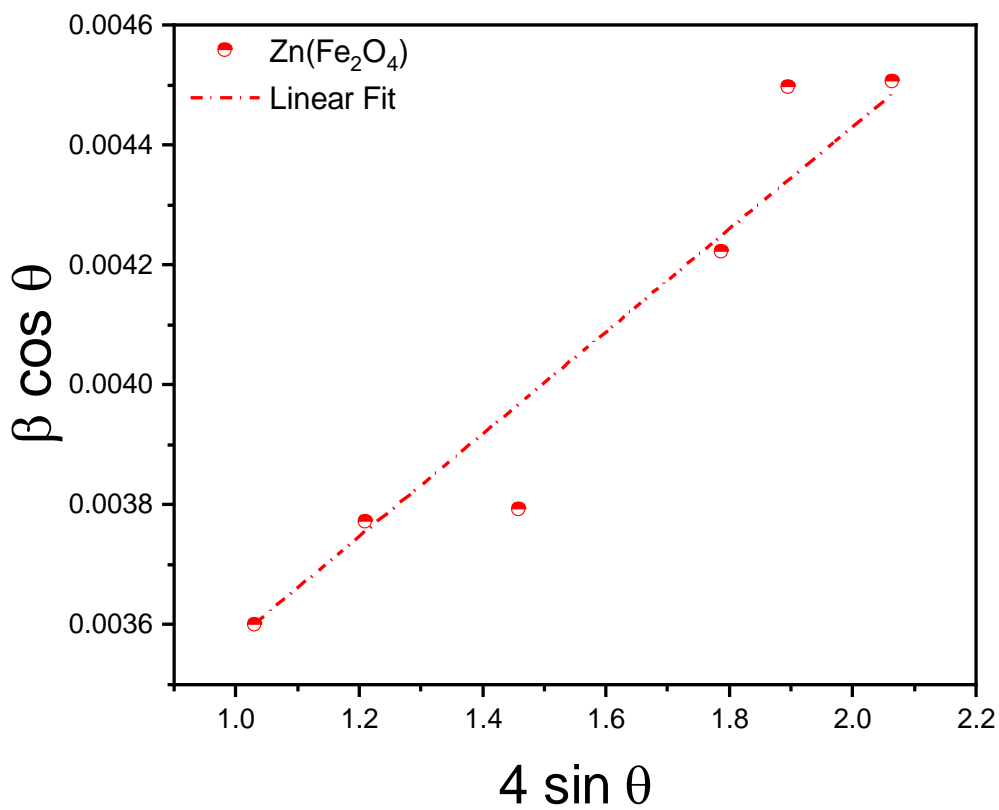Figure 4.5: Linear curve showing Williamson Hall plot for zinc oxide

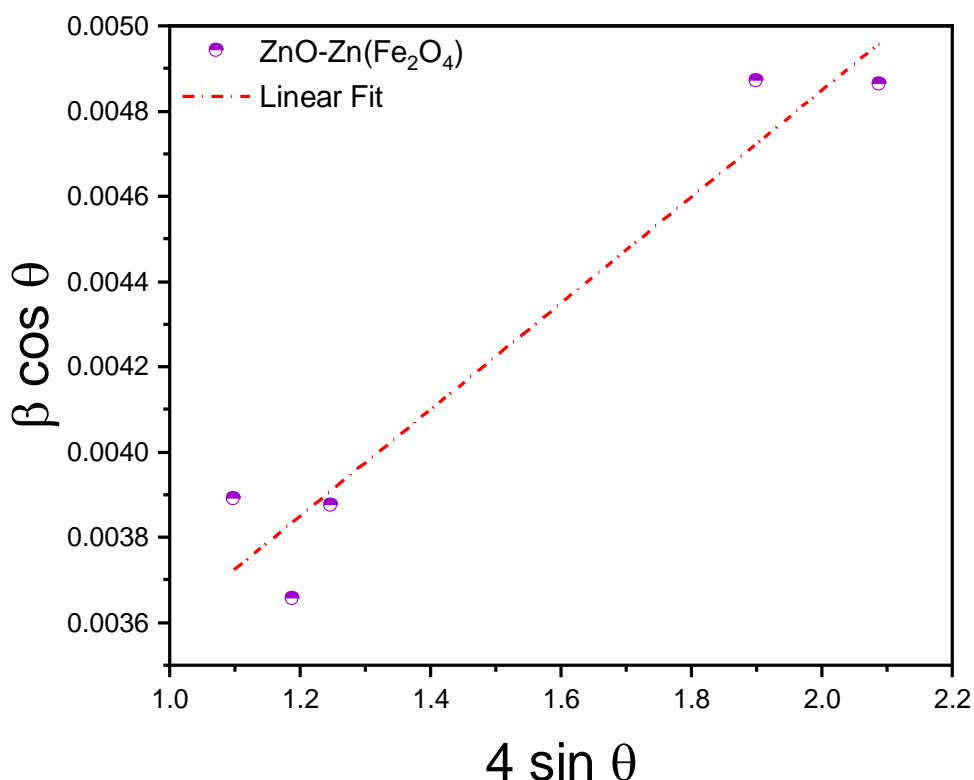Figure 4.4: Linear curve showing Williamson Hall plot for zinc ferrite

Figure 4.6: Linear curve showing Williamson Hall plot for composite material

The average crystallite size D for ZnO particles is found to be 34.41nm whereas for Zinc ferrite it is 38.38 nm. The average crystallite size for ZnO-Zn(Fe$_2$O$_4$) composite is 26.33 nm.

4.1.2 FTIR Analysis

Fourier-transform infrared spectroscopy (FTIR) spectra of three samples was obtained using FTIR spectrometer. The technique used for sample preparation was KBr method and it was measured at 4000 cm^{-1} to 400 cm^{-1} scale range. The sample was analyzed in solid form. The pellets of the sample were made by blending the magnetite sample with potassium bromide in a ratio of 1:200 (wt/wt) , respectively. The number of scans in the scanned sample were 32 cm^{-1} and the range was set to 4 cm^{-1}.

4.1.2.1 FTIR spectrum for ZnO

The FTIR spectrum of ZnO shows absorption bands around 491 cm^{-1} and 840 cm^{-1}, which are characteristic of Zn-O stretching vibrations. The presence of these bands confirms the successful synthesis of ZnO.
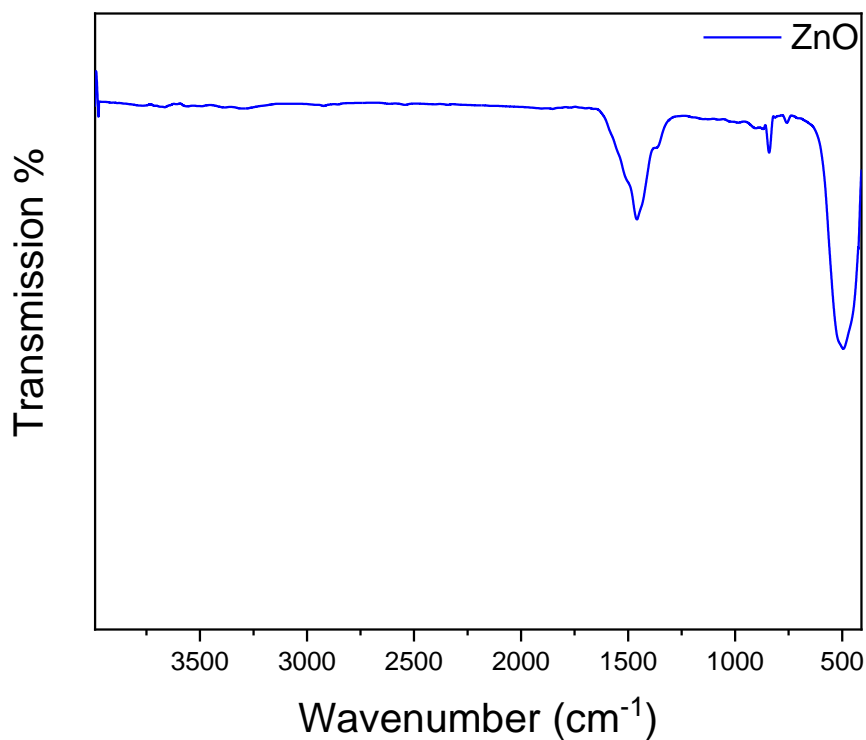
Figure 4.7: FTIR spectrum for zinc oxide

4.1.2.2   FTIR spectrum for Zn(Fe₂O₄)

The following graph shows FTIR spectrum for $Zn(Fe_2O_4)$ which shows bands around 1650 cm⁻¹ and 1414 cm⁻¹, corresponding to the Fe-O and Zn-O-Fe bond
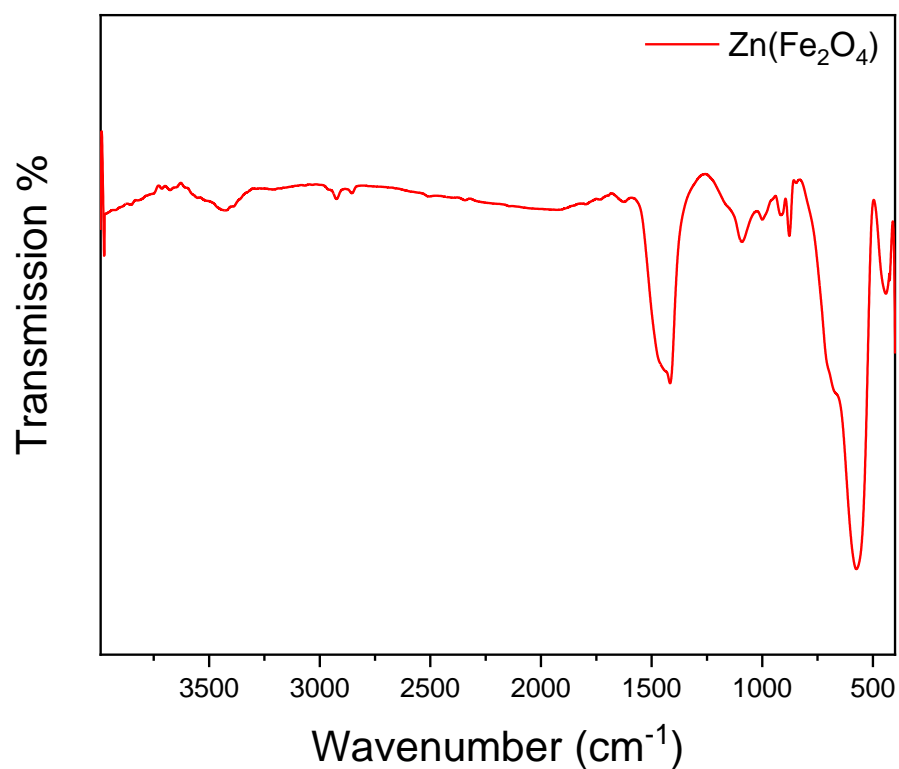
Figure 4.8: FTIR spectrum for zinc ferrite

45

vibrations, respectively. These peaks confirm the formation of the ferrite phase in the material.

4.1.2.3   FTIR spectrum for ZnO-Zn(Fe₂O₄) composite

The FTIR spectra of the ZnO- $Zn(Fe_2O_4)$ composite show characteristic absorption bands of both ZnO and $Zn(Fe_2O_4)$ The spectrum confirms the presence of
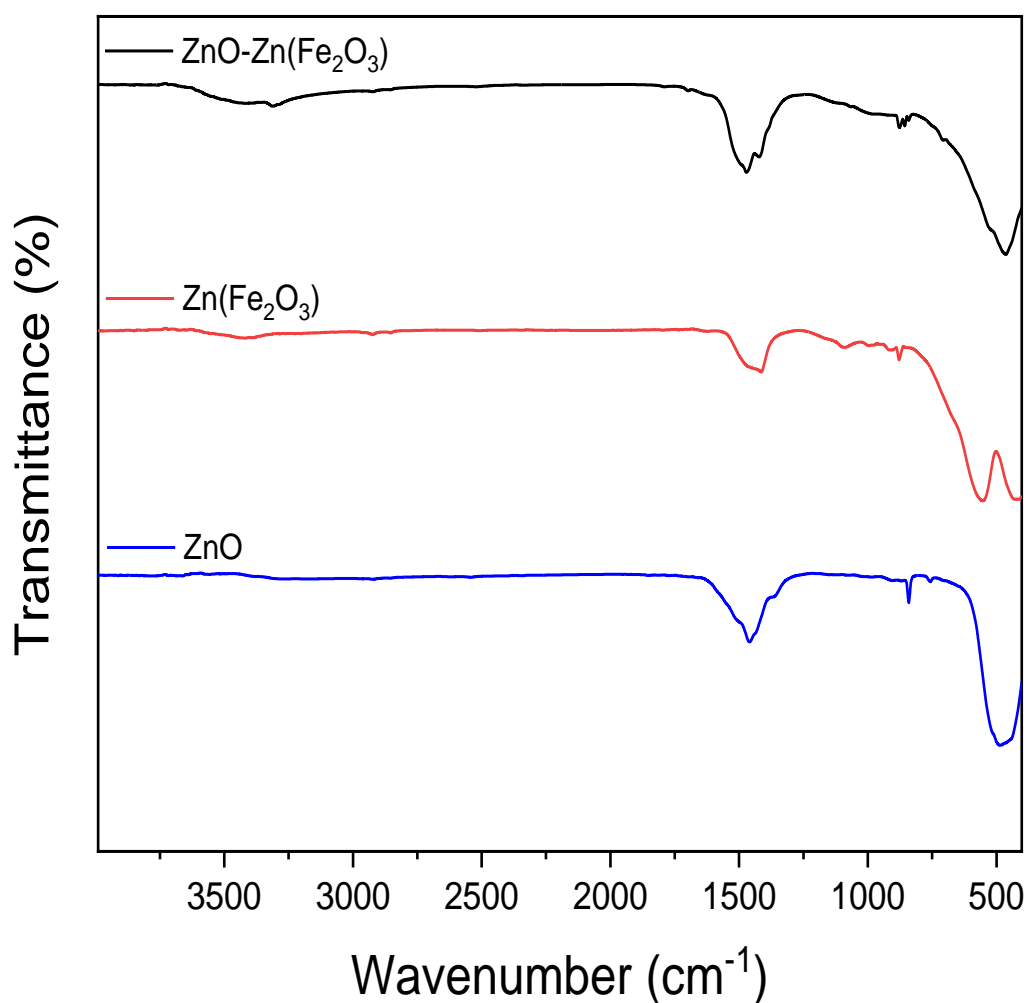
Figure 4.9: FTIR spectrum for zinc oxide, zinc ferrite and composite material

both phases, as indicated by the respective peaks in the ZnO (blue) and $Zn(Fe_2O_4)$ (red) spectra. The composite's spectrum indicates successful integration of both components without any significant chemical interaction or degradation.

4.1.3 SEM Analysis

`   The morphological study of the synthesized material was carried out by SEM. The average diameter of particles is found by using Gaussian distribution function.

Table 4.2: Table showing average diameters for particles

Material	Average Diameter
Zinc Oxide	0.25 µm
Zinc Ferrite	0.19 µm
ZnO-$Zn(Fe_2O_4)$ (Composite)	0.22 µm

4.1.3.1 ZnO

The SEM analysis was performed to analyze the shape, structure and size of synthesized nanoparticles (Fakhari et al., 2019). It can be seen that spherical shaped agglomerated structures are formed that are uniformly distributed and varies in shape and size. Co-precipitation method was used which resulted in the formation of spherical particles.
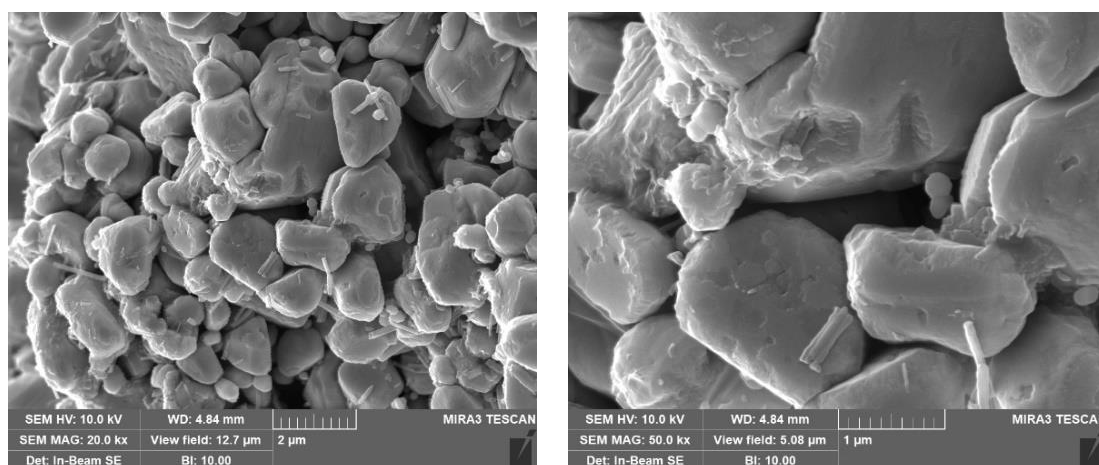
Figure 4.10: SEM monographs of zinc oxide

The average size of ZnO nanoparticles is found to be 0.25 µm. The particle size distribution for ZnO particles is shown in distribution graph.
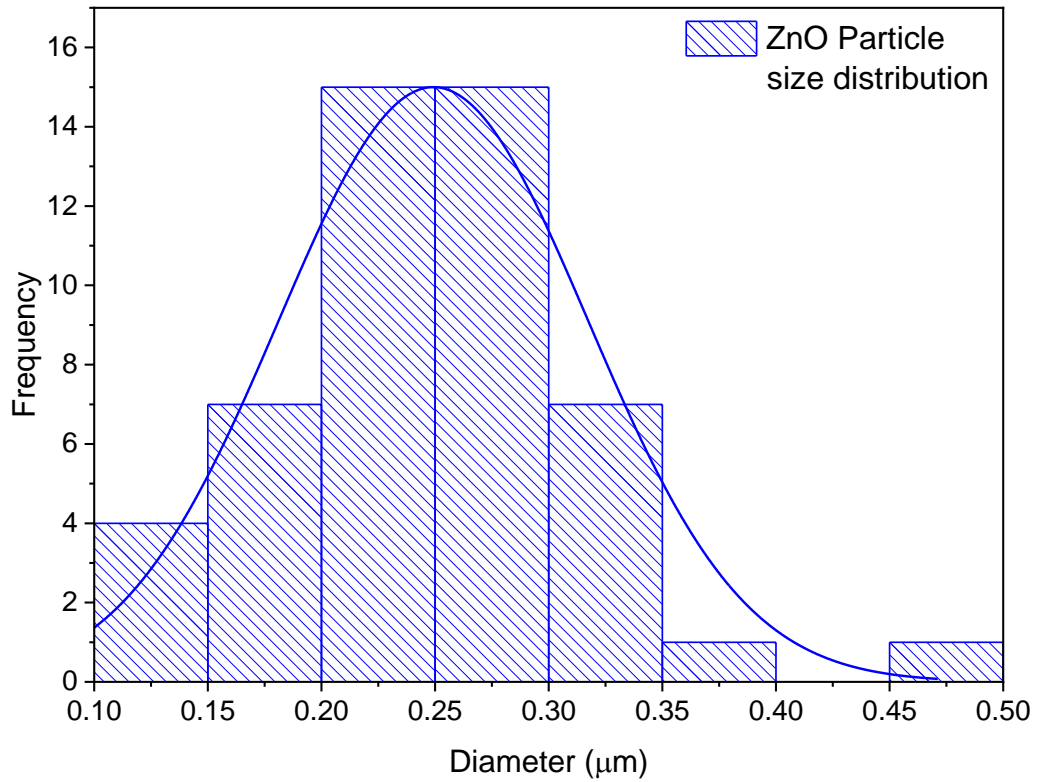
Figure 4.11: Graph showing particle size distribution for zinc oxide particles

4.1.3.2 *Zn(Fe₂O₄)*

SEM analysis of $Zn(Fe_2O_4)$ particles showed the morphological structure. The following image shows the SEM micrographs at different magnifications. The figure represents the presence of large agglomerated particles having polyhedral crystal like shape (Liu et al., 2019). The average diameter of $Zn(Fe_2O_4)$ particles is found to be 1.96 µm.
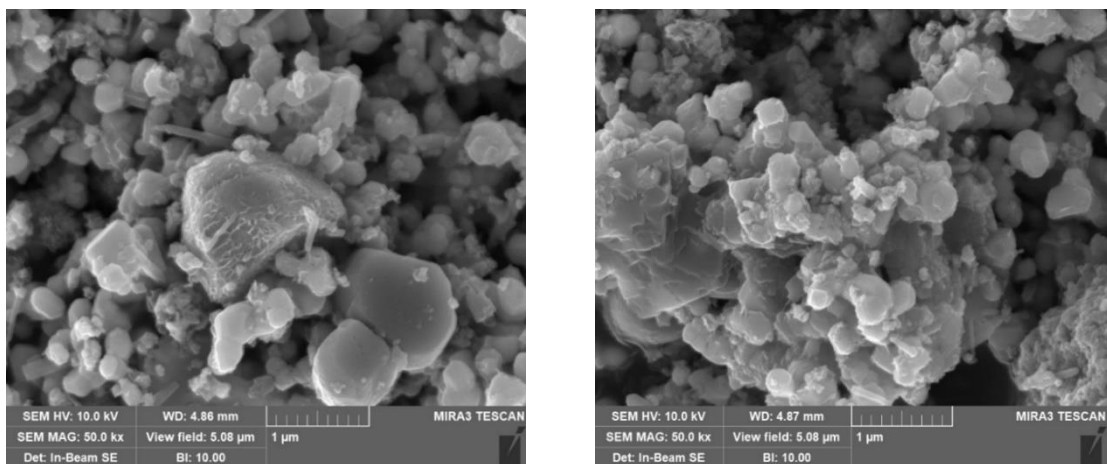
Figure 4.12: SEM monographs for zinc ferrite particles
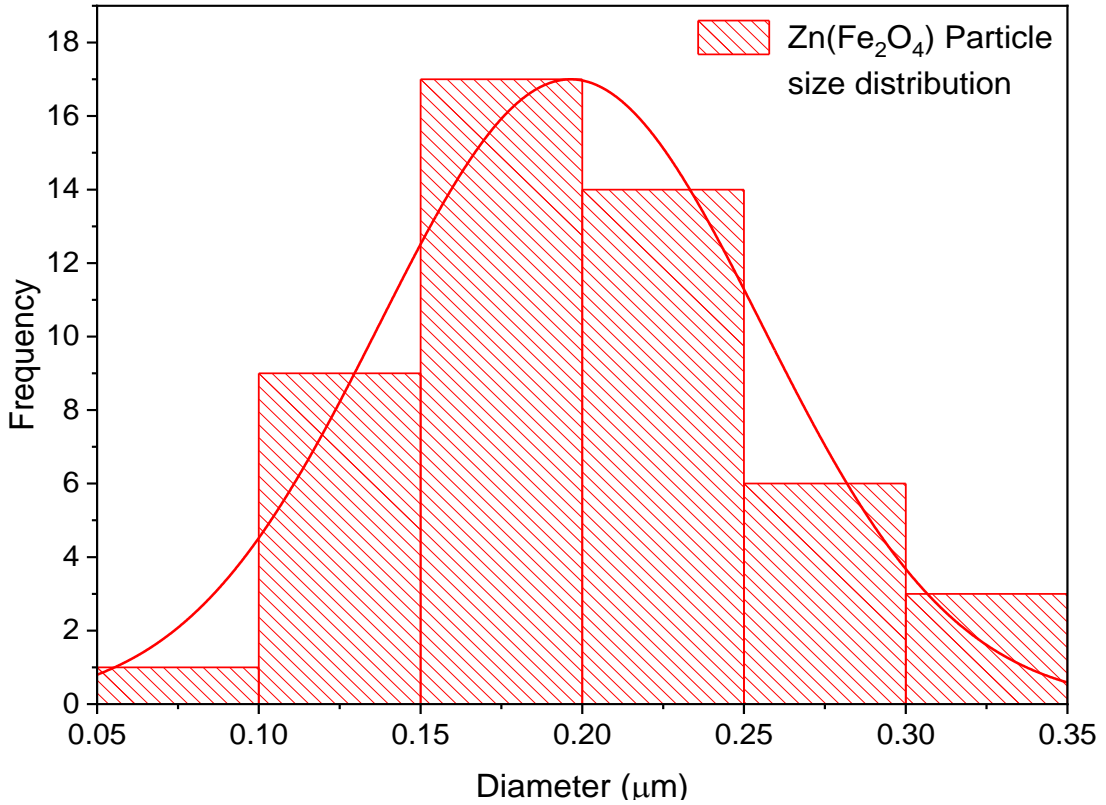
Figure 4.13: Graph showing particle size distribution for zinc ferrite

4.1.3.3 Composite

The SEM of composite confirms the presence of both ZnO and $Zn(Fe_2O_4)$ nanoparticles. Mixture of agglomerated grain like and polyhedral structures confirms the presence of both particles. The histogram below shows the average particles size distribution for these particle. The average particle size for composite is found to be 0.22 µm.
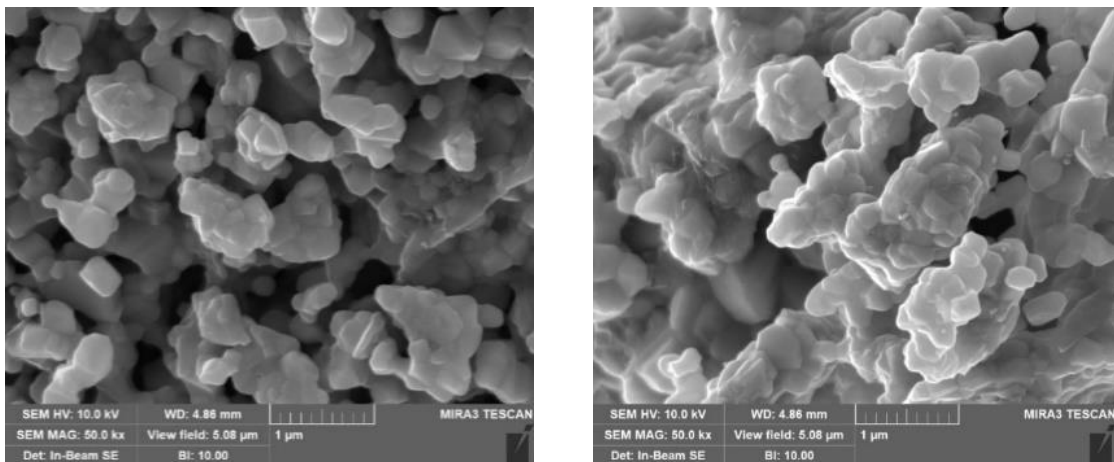
Figure 4.14: SEM monographs of zinc oxide and zinc ferrite composite
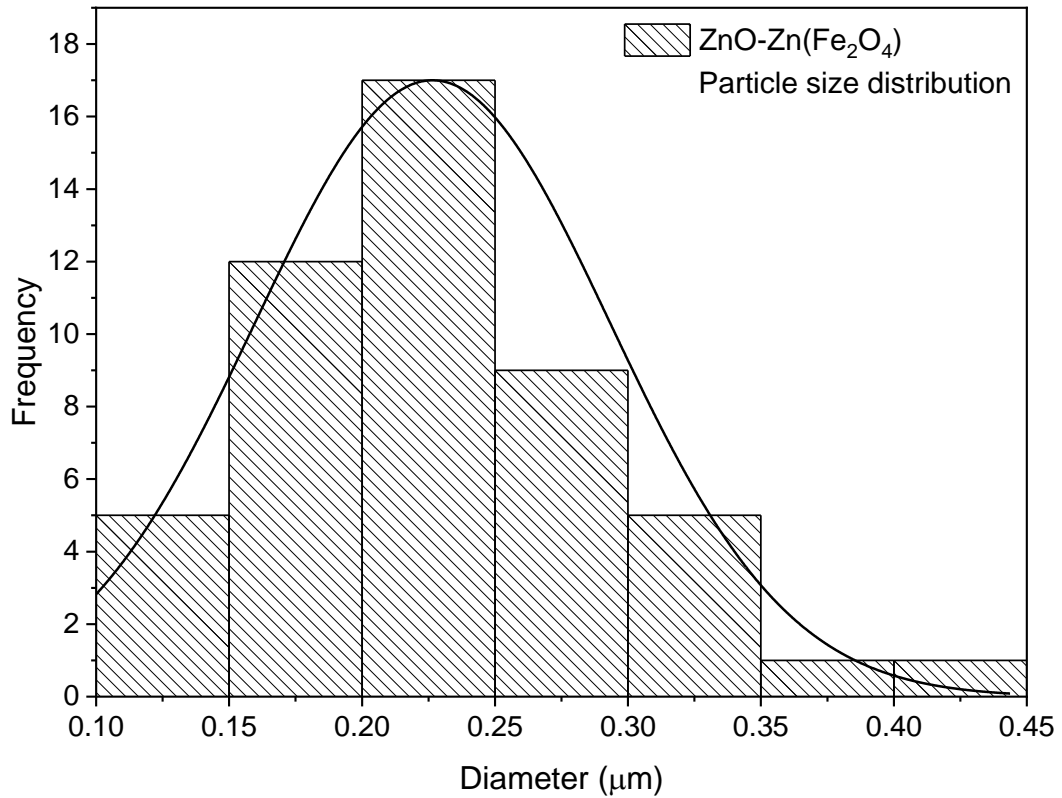
Figure 4.15: Graph showing particle size distribution for zinc oxide and zinc ferrite composite

4.1.4   EDS Analysis

4.1.4.1   ZnO

The EDS pattern shows that majority particles are of Zn and second highest number of particles are O which shows the successful preparation of ZnO. The presence of zinc (Zn) and oxygen (O) in the sample, as indicated by the peaks in the EDS spectrum. This confirms the elemental composition of ZnO.
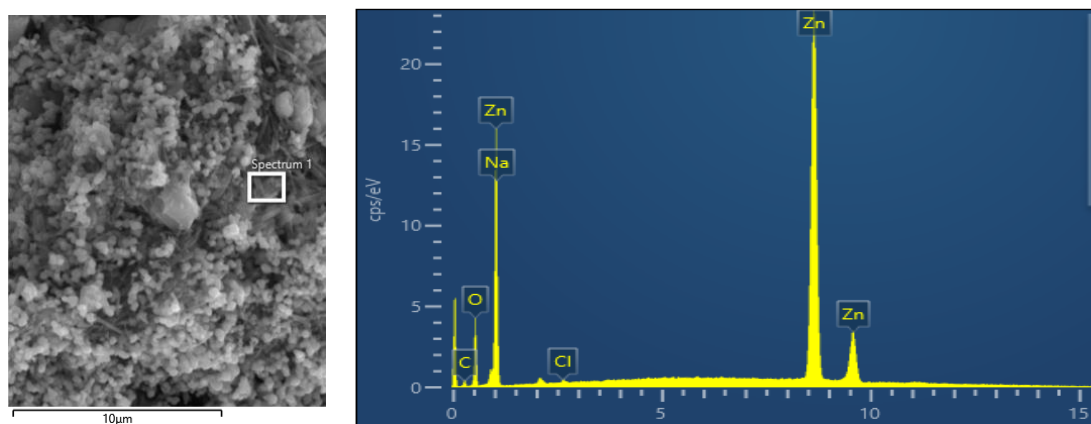
Figure 4.16: EDX spectrum for zinc oxide

The table shows the detailed content analysis of components found. It shows the atomic percentage of Zn and oxygen which is 90:4.

Table 4.3: Elemental composition of synthesized zinc oxide using EDS analysis by weight percentage

Spectrum Label	Spectrum 1
O	4.06
Na	4.01
Cl	0.09
Zn	90.05
Total	**100.00**

4.1.4.2 *Zn(Fe$_2$O$_4$)*

The EDS patterns show the highest percentage of Zn and Fe which confirms the formation of Zn(Fe$_2$O$_4$). The energy dispersive X-ray spectrum shows the composition ratio of Zinc and ferrite approximately same as it was considered during the synthesis phase. The peaks corresponding to zinc (Zn), iron (Fe), and oxygen (O), confirming the successful synthesis of the Zn(Fe$_2$O$_4$) phase. The presence of these elements supports the formation of the spinel structure. A negligible amount of Ca and Si are found which may be left due to improper washing (Basavanagoudra et al., 2021).
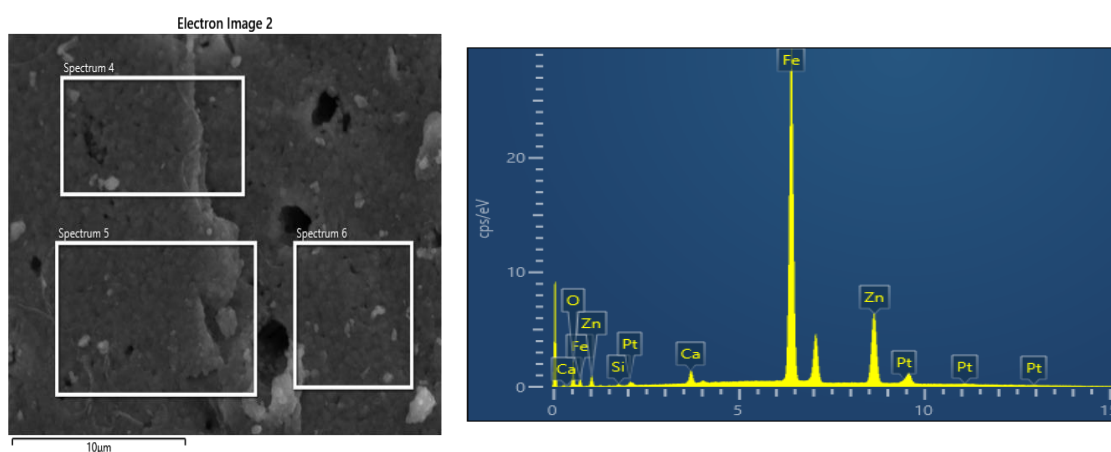
Figure 4.17: EDX spectrum for zinc ferrite

Table 4.4: Elemental composition of synthesized zinc ferrite using EDS analysis by weight percentage

Spectrum Label	Spectrum 6
O	2.27
Si	0.12
Ca	0.89
Fe	62.21
Zn	34.51
Total	**100.00**

4.1.4.3 Composite

The EDS of the composite material shows that it has highest percentage of Zn, Fe and O respectively. The composite shows the presence of all relevant elements: Zn, Fe, and O. This indicates the successful combination of ZnO and $Zn(Fe_2O_4)$ in the composite material. The distribution of elements also suggests uniform mixing of the two phases. Some other materials are also observed in minute quantity which shows impurities due to improper Washing. The purity of material formed in 93%.
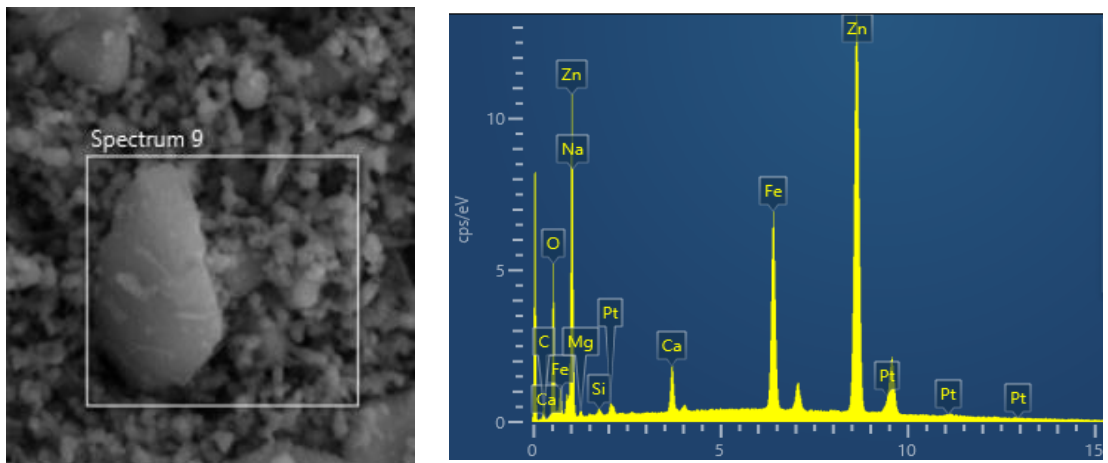
Figure 4.18: EDX spectrum for composite material

The table below shows the elemental composition for $Zn)-Zn(Fe_2O_4)$ composite material.

Table 4.5: Elemental composition of synthesized Composite using EDS analysis by weight %

Spectrum Label	Spectrum 9
C	3.08
O	6.76
Na	2.77
Mg	0.34
Si	0.16
Ca	1.33
Fe	13.36
Zn	72.20
Total	**100.00**

4.1.5 BET Analysis

Brunaeur Emmett Teller analysis was performed to analyze the surface area and porosity of material. In the case of a Type III isotherm, there is no Point B and therefore no identifiable monolayer is formed. The adsorbent-adsorbate interactions are relatively weak and the adsorbed molecules are clustered around the most favorable sites on the surface of a nonporous or macro-porous solid.

Table 4.6: Table depicting surface area, pore volume and pore diameter for three materials

BET Analysis			
Parameters			
Material	**BET Surface Area**	**Average Pore Volume**	**Average Pore Diameter**
ZnO	2.49 m²/g	0.008 cm³/g	16.29 nm
$Zn(Fe_2O_4)$	2.12 m²/g	0.0145 cm³/g	40.17 nm
ZnO- $Zn(Fe_2O_4)$	10.37 m²/g	0.0604 cm³/g	23.97 nm

The BET (Brunauer-Emmett-Teller) analysis shows that ZnO has a relatively small surface area and small pores whereas $Zn(Fe_2O_4)$ has a higher BET surface area of 2.12 m²/g with a larger pore volume of 0.0145 cm³/g and an average pore diameter of 40.17 nm. The composite shows the highest BET surface area of 10.39 m²/g, with a pore volume of 0.008 cm³/g and an average pore diameter of 23.97 nm.
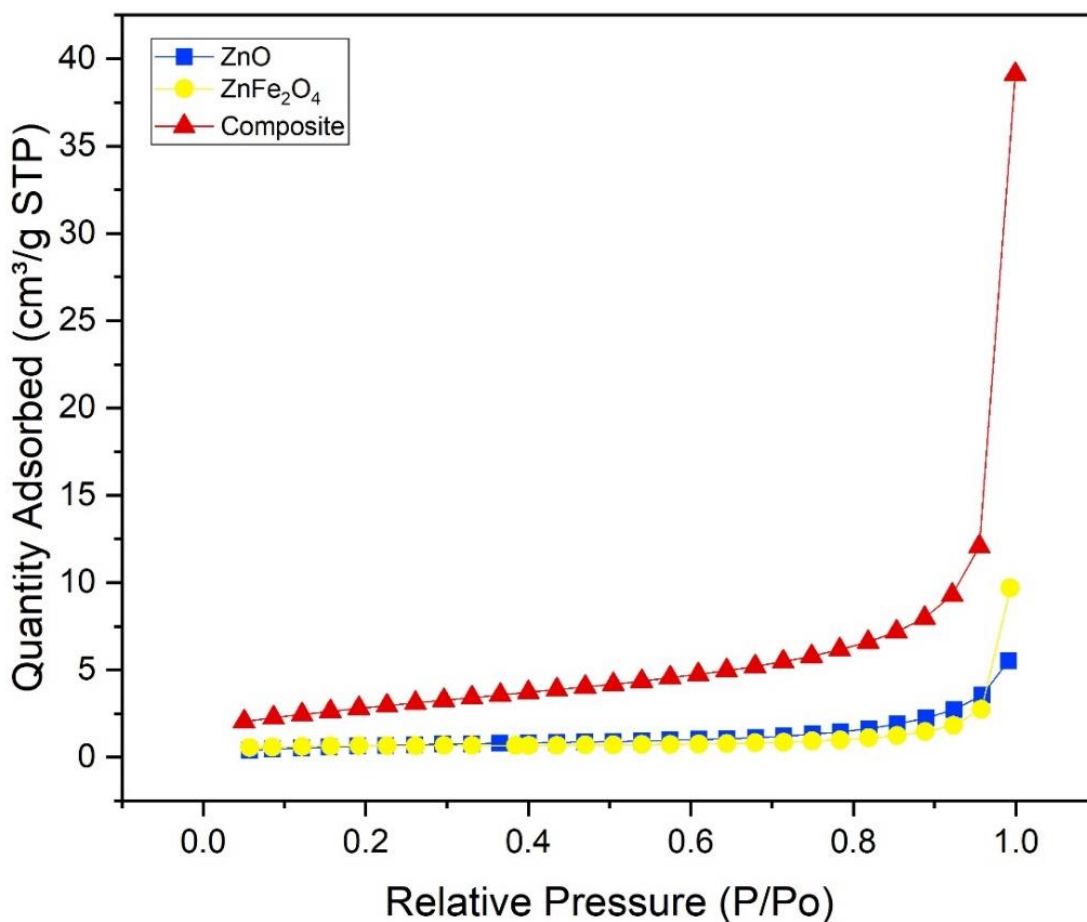
Figure 4.19: Graph showing adsorption curve for zinc oxide, zinc ferrite and composite material

4.1.6 RAMAN Analysis

Raman analysis is used to study the rotational, vibrational and other low frequency modes in particles. It gives a useful information about crystallinity, bonding and molecular structure of synthesized particles.

4.1.6.1 ZnO

The Raman spectrum of ZnO shows several characteristic peaks that correspond to its phonon modes, which confirms the hexagonal wurtzite crystal structure. E_2 (Low) mode near ~100 cm^{-1} shows low-energy mode which is due to the non-polar modes of ZnO; the primary confined motions are the oscillations of the oxygen atoms. E_2 (High) mode at ~439 cm^{-1} is the most intense bonding in the ZnO spectrum and is associated with the vibration of the oxygen atoms in the lattice. A_1 (LO) mode at ~581 cm^{-1} is associated with lattice vibrations and is attributed to oxygen losses or to defects in the ZnO lattice. Thus, the Raman spectrum of ZnO proves its wurtzite structure and the presence of defects, such as oxygen vacancies.
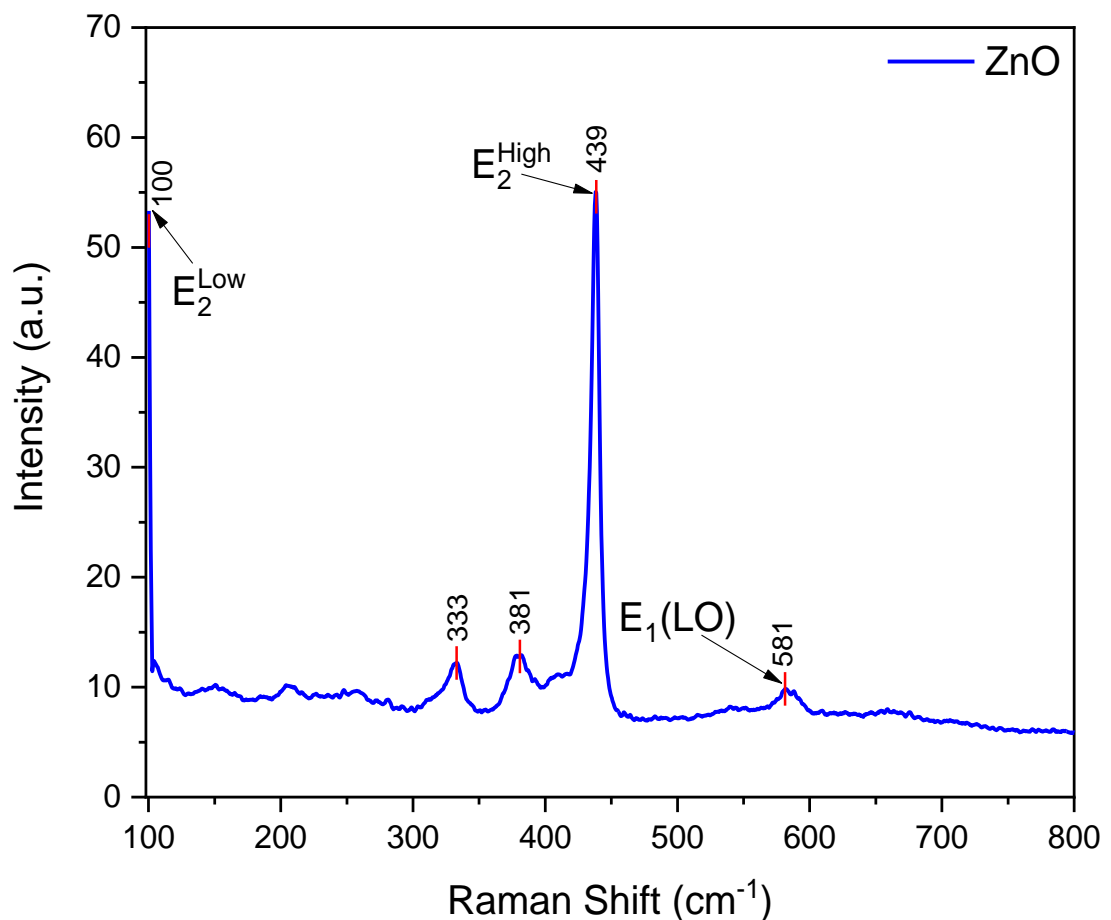
Figure 4.20: RAMAN graph for zinc oxide

4.1.6.2 $Zn(Fe_2O_4)$

The Raman spectrum of $Zn(Fe_2O_4)$ shows peaks that correspond to the vibrational modes typical of spinel structures. E_g mode around ~315 cm^{-1} has been related to the symmetric stretching vibration of the Fe-O bonds at the tetrahedral site of the spinel structure. F_{2g} (2) mode around ~380 cm^{-1} concerns the change in the Fe-O bond lengths in the tetrahedral and octahedral positions of the spinel structure. F_{2g} (3) mode at ~500 cm^{-1} is particularly assigned to the vibrational modes of the Fe-O. A_{1g} mode at ~690 cm^{-1} is the most intense peak and the bands are assigned to the symmetric stretching vibrations of oxygen atoms in the Fe-O octahedral groups. The high peak intensity in Raman spectrum of $Zn(Fe_2O_4)$ indicates its spinel crystal structure and high intensity peaks corresponds to vibrational modes of the metal-oxygen bonds. This shows evidence of the ferrite structure synthesis with good crystalline nature of the materials attained.
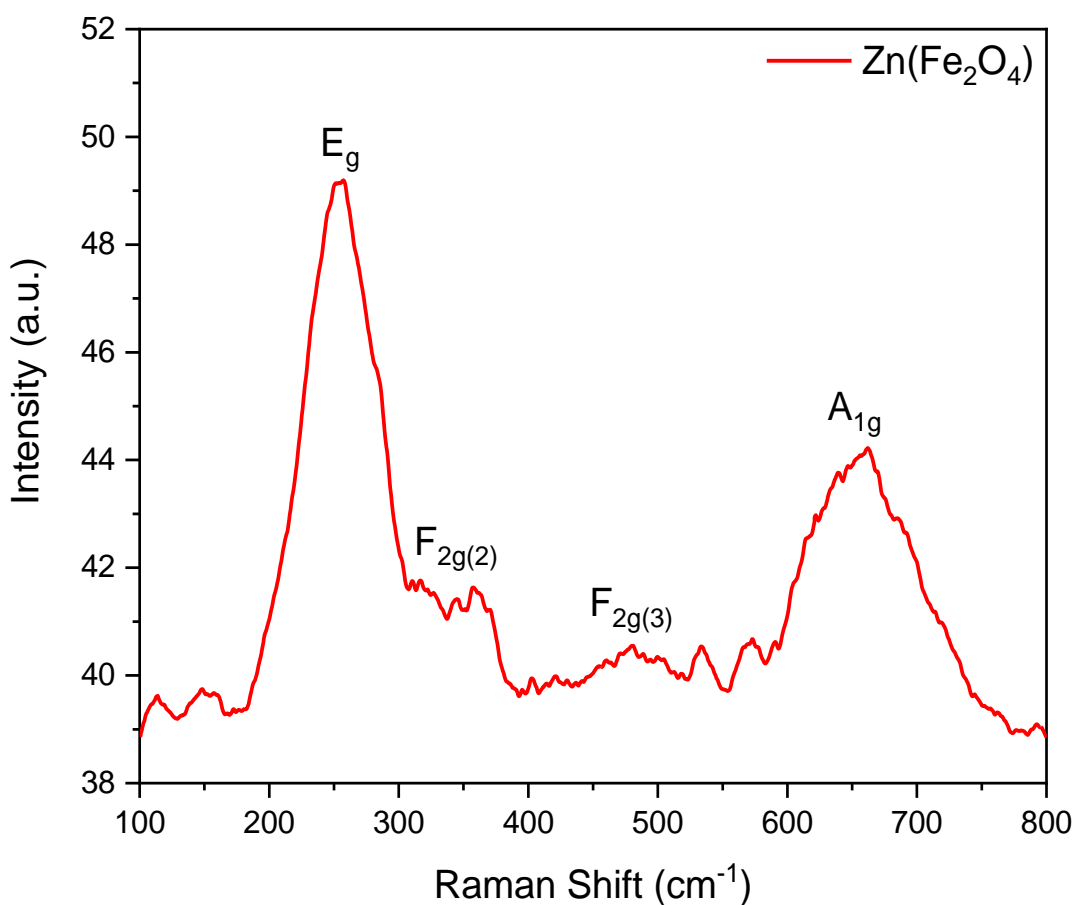
Figure 4.21: RAMAN graph for zinc ferrite

4.1.6.3 Composite

In the composite spectrum, the broadening of the peaks and the shift of the intensity is clearly seen. These broadening show that there is little diffusion of ZnO and $Zn(Fe_2O_4)$ interfaces and therefore there is a good interfacial contact between the two materials at the nanometer scale. The maxima observed at ~ 100 cm^{-1} is assigned to the E_2 low mode of ZnO and the maxima at ~ 660 cm^{-1} may be attributed to the A_1g mode of zinc ferrite. An evidence for such interaction is the decrease of the intensity of the E_2(high) mode (~ 437 cm^{-1}) of ZnO in the composite as compared to the intensity of this mode in ZnO without interaction with $Zn(Fe_2O_4)$.
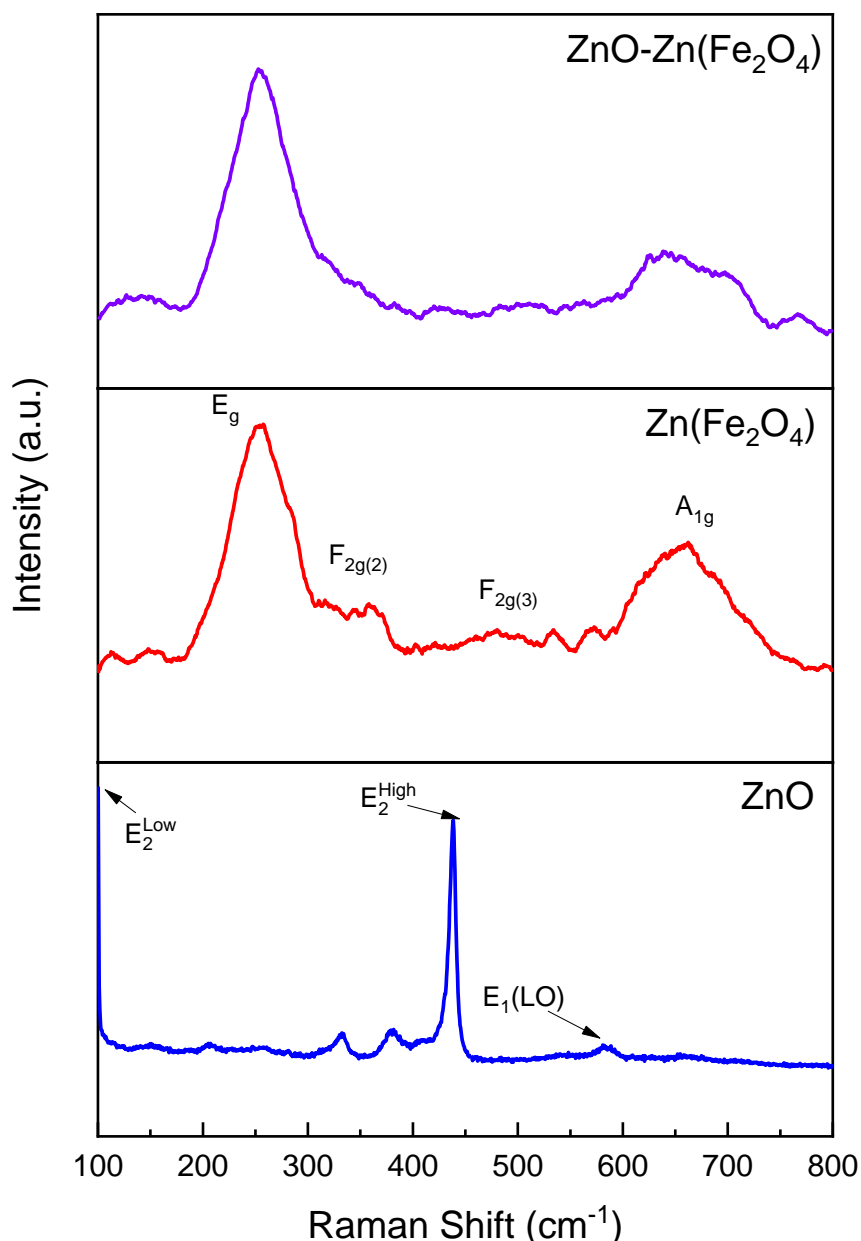
Figure 4.22: RAMAN curves for zinc oxide, zinc ferrite and composite material

57

4.1.7 VSM analysis

VSM is used to study the magnetic behavior of materials by measuring their magnetic moment as a function of an applied magnetic field. In this graph we see that Zinc oxide has decreased magnetic behavior as compared to zinc ferrite. Composite shows super paramagnetic behavior.
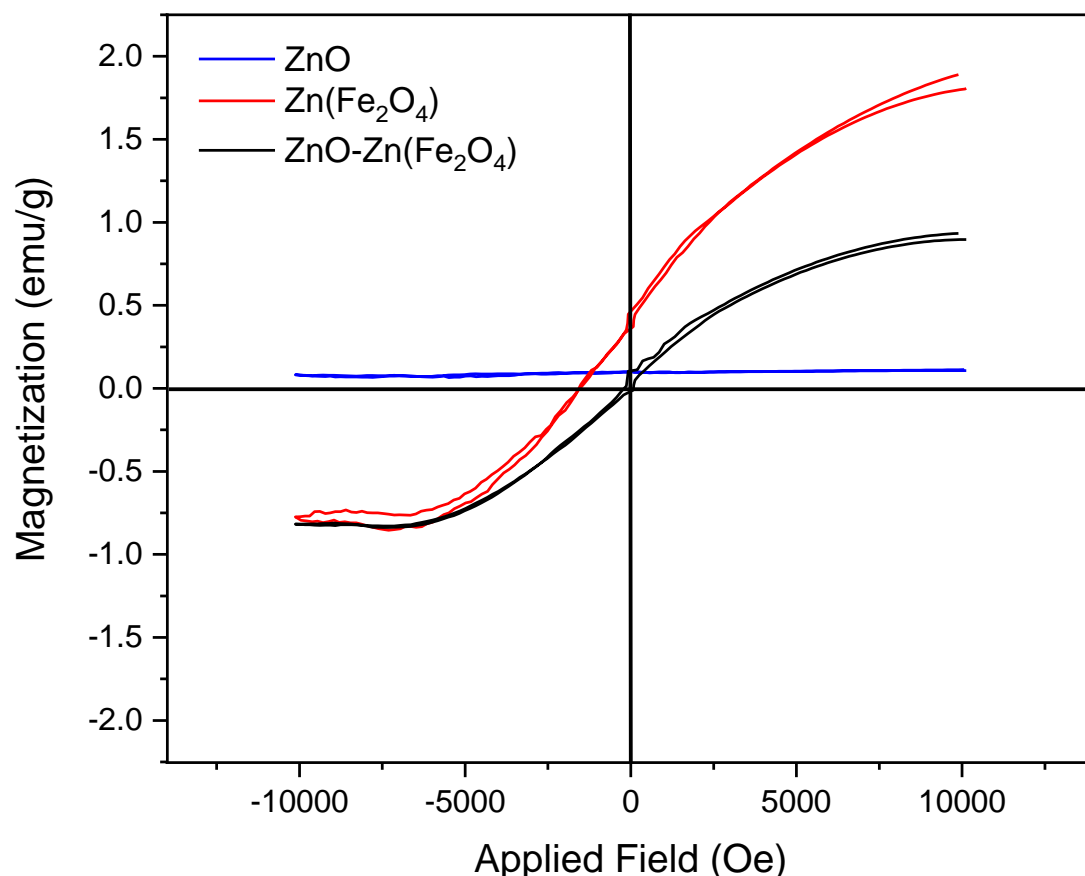
Figure 4.23: Hysterical loop for all three materials showing their magnetic properties

4.2 Degradation Analysis

The key objectives of this work is to utilize the synthesized ZnO and $Zn(Fe_2O_4)$ nanocomposites for the photodegradation of methylene blue, which is a toxic chemical commonly found in wastewater from the textile sector. The photocatalytic degradation activity of synthesized ZnO and $Zn(Fe_2O_4)$ was investigated under visible irradiation. The theory of semiconductor-based photocatalysis holds that the surface area, band gap, morphology, crystallinity, particle size and the concentration of OH • free radicals on the surface of a photocatalyst is directly proportional to its photocatalytic efficiency. When light is absorbed, there are electrons and holes on the surface of the semiconductor, and these electrons and holes would join in a reaction or recombine.

The light source, photocatalyst dose, dye concentration, irradiation time, and pH are factors considered during this experiment, and the MB was chosen as the reference pollutant for the photocatalytic degradation in the investigation. Finally, to support the results attained, variation in the intensity of the absorption peak recorded at 665 nm (λ_{max} MB) was analyzed. The calibration curve of methylene blue was obtained and R~1 shows the accuracy of obtained calibration curve.
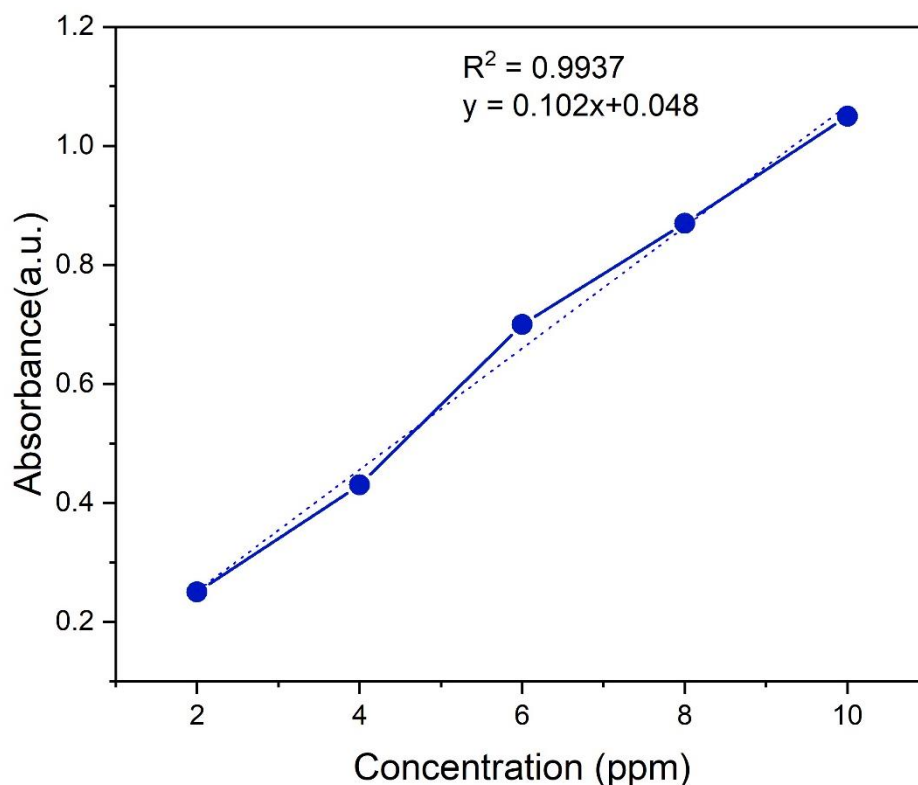
Figure 4.24: Calibration curve for methylene blue dye degradation

4.2.1 Photocatalytic Degradation of Methylene blue by ZnO

The photocatalytic degradation of methylene blue was carried out in photocatalytic chamber under visible light. The degradation experiment was carried out for 80 minutes under visible radiation and samples were obtained consecutively after every 20 minutes. The samples absorbance was measured by UV-vis spectrophotometer and change in absorbance over the period of time was plotted on absorbance spectra. The degradation experiment was carried out under dark and light conditions under the presence of ZnO

Figure 4.25: Absorbance spectra for methylene blue degradation under dark conditions in presence of zinc oxide

Figure 4.26: Absorbance spectra for methylene blue degradation under light conditions in presence of zinc oxide

as photocatalyst. The absorbance spectra showed decrease in absorbance over the period of time in presence of light which depicts the successful degradation of MB by ZnO.

4.2.2 Photocatalytic Degradation of Methylene blue by $Zn(Fe_2O_4)$

The photocatalytic degradation of MB was carried out in photocatalytic chamber under visible light in presence of zinc ferrite as photocatalyst. The degradation experiment was carried out for 120 minutes under visible radiation and samples were obtained consecutively after every 20 minutes. The samples absorbance was measured by UV-vis spectrophotometer and change in absorbance over the period of time was plotted on absorbance spectra. The degradation experiment was carried out under dark and light conditions under the presence of $Zn(Fe_2O_4)$ as photocatalyst. The absorbance spectra showed decrease in absorbance over the period of time in presence of light which depicts the successful degradation of MB by $Zn(Fe_2O_4)$.
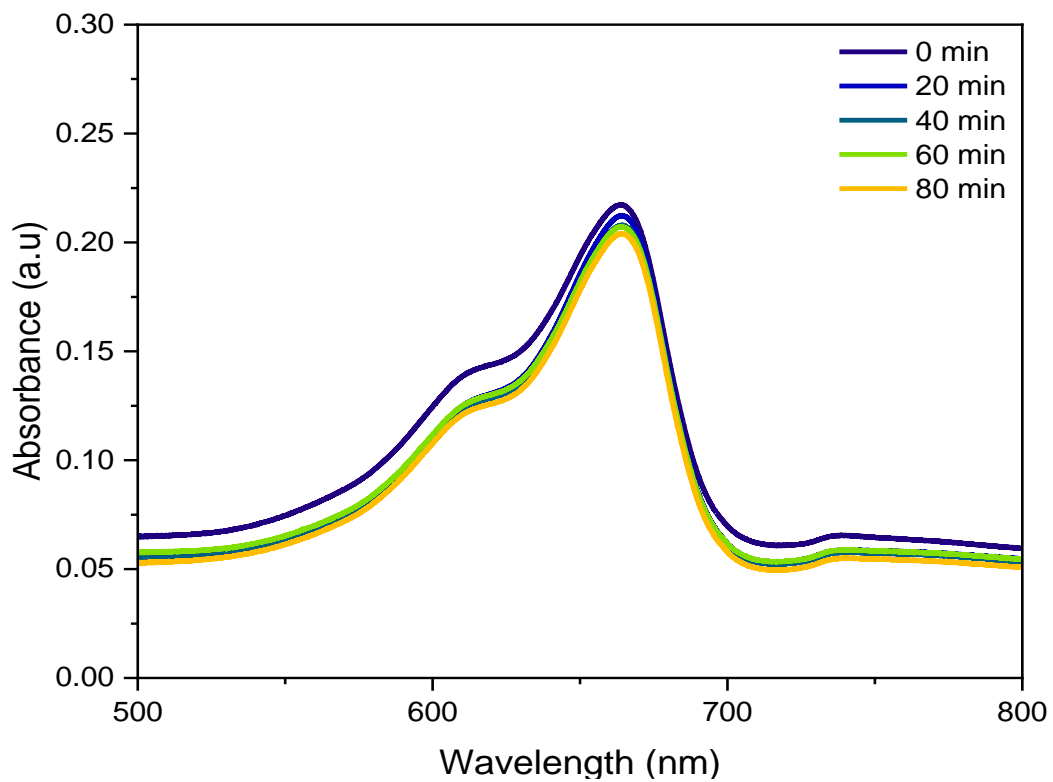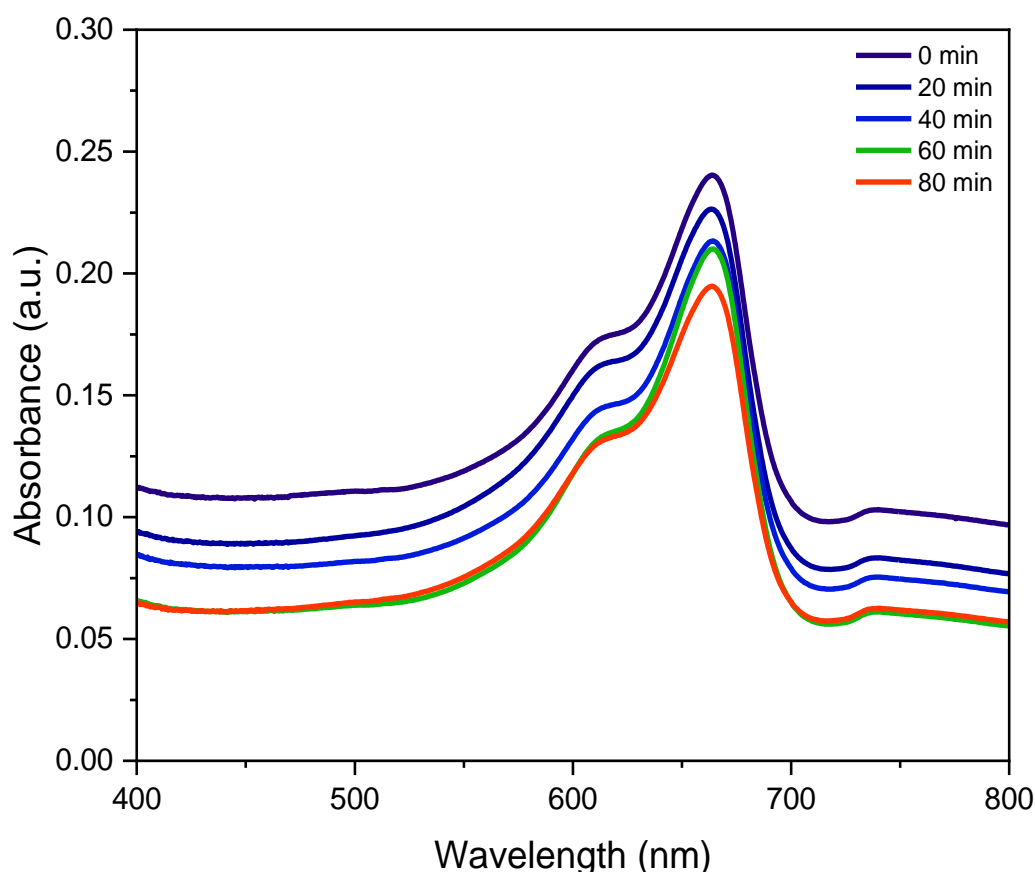

Figure 4.27: Absorbance spectra for methylene blue degradation under dark conditions in presence of zinc ferrite
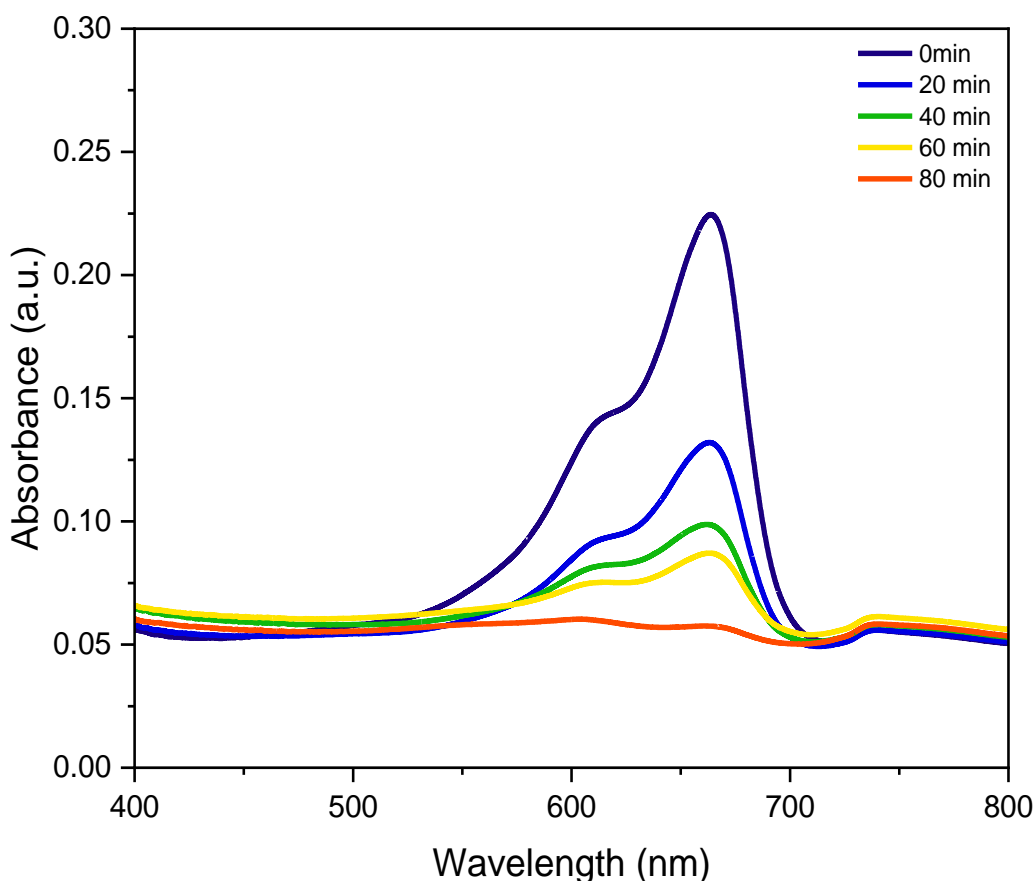
Figure 4.28: Absorbance spectra for methylene blue degradation under light conditions in presence of zinc ferrite
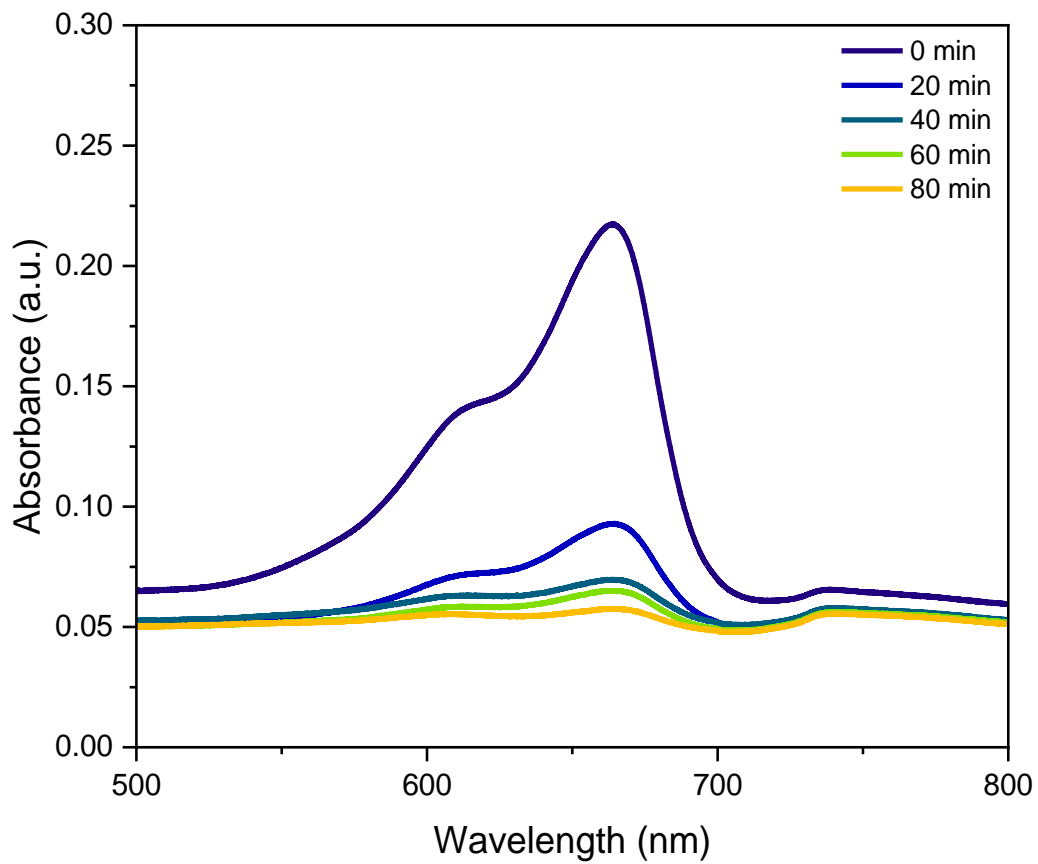
4.2.3 Photocatalytic Degradation of Methylene blue by ZnO-Zn(Fe$_2$O$_4$) composite

The degradation of MB was carried out in photocatalytic chamber under visible light in presence of ZnO-Zn(Fe$_2$O$_4$) composite. The degradation experiment was carried out for 80 minutes under visible radiation and samples were obtained consecutively after every 20 minutes. The samples absorbance was measured by UV-vis spectrophotometer and change in absorbance over the period of time was plotted on absorbance spectra. The absorbance spectra showed decrease in absorbance over the period of time in presence of light which depicts the successful degradation of MB by ZnO-Zn(Fe$_2$O$_4$). The purpose of using composite as a photocatalyst is to evaluate the performance of both materials synergistical way.

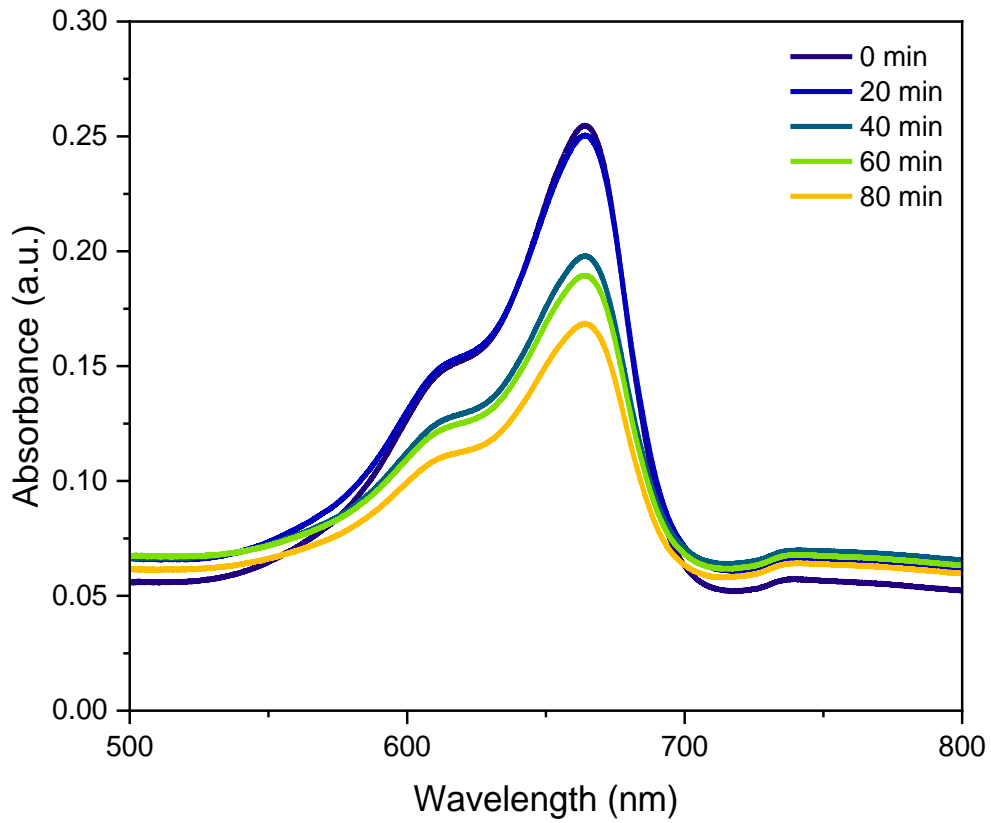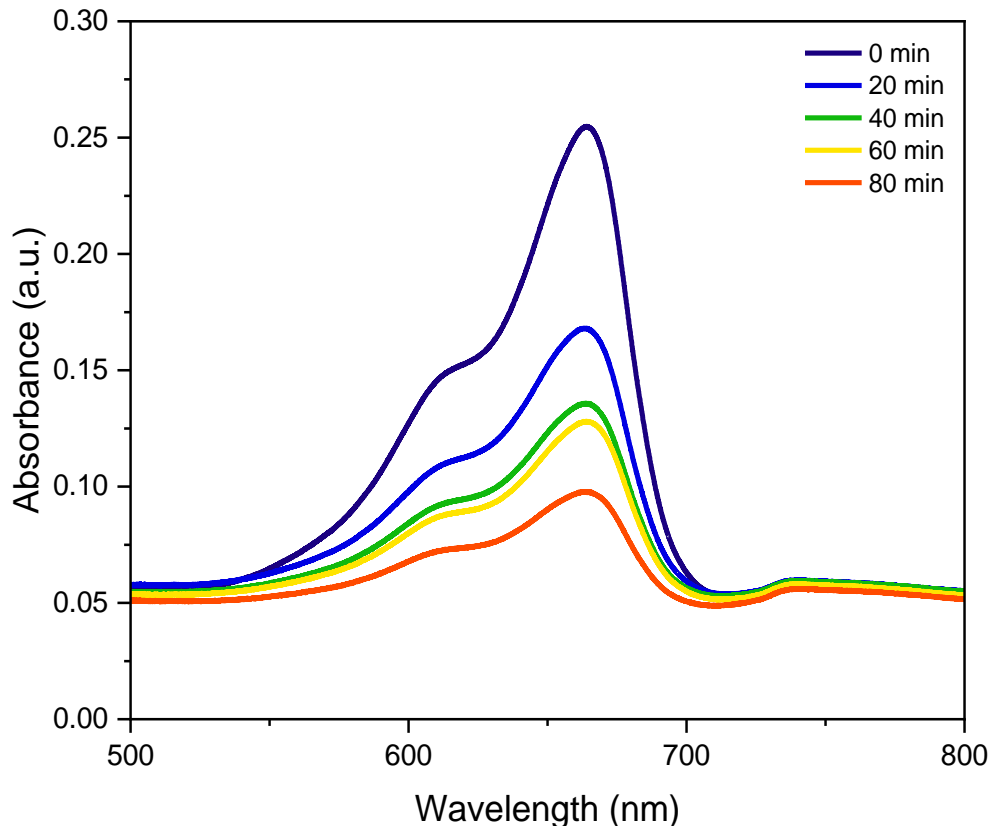Figure 4.29: Absorbance spectra for methylene blue degradation under dark conditions in presence of ZnO-Zn(Fe$_2$O$_4$) composite

Figure 4.30: Absorbance spectra for methylene blue degradation under light conditions in presence of ZnO-Zn(Fe$_2$O$_4$) composite

4.3   Reaction Kinetics

In order to understand the degradation mechanism, it is very necessary to analyze the reaction mechanism. For this purpose, reaction kinetics are being studied. The first graph depicts the degradation of MB in three different processes in the presence of catalyst. It shows the photodegradation, adsorption and photocatalytic behavior of MB. The red curve indicates influence of light on the degradation of MB in absence of the catalyst. In 120 minutes, the concentration of MB is reduced a little proving that light without the use of anything else does break down MB at a small rate, a form of photodegradation. The decrease in the value of C/Co over time indicates that even light seems not to be very efficient in the degradation of MB in the absence of a catalyst.

The black curve show the MB adsorption onto the surface of catalyst in dark condition. The nearly constant trend depicted by the curve implies that ZnO has moderate adsorption ability for MB and its C/Co value is constantly around 1.0. The adsorption contribution to the overall MB removal is very small and hence in the dark, the catalyst does not adsorb much of the MB.

The blue curve represents the degradation of MB using catalyst under light. The concentration (C/Co) decreases dramatically and declines to very low levels within the first 60 minutes and further after 120 minutes. This points to the efficiency of synthesized catalyst as a photocatalyst when exposed to light since the rate of degradation of MB is significantly enhanced to near 95-98% degradation of the dye. From this graph it is clearly evident that, MB degrades much faster in the presence of catalyst under light compared to the individual effect of photodegradation and adsorption.

The second graph shows the reaction kinetics for MB degradation in the presence of 3 different materials. The higher R^2 value shows that the data fits the linear model and hence the process follows pseudo 1st order reaction kinetics, which is shown as follows:

$$\ln \frac{C}{C_o} = kt$$

Figure 4.31 Methylene blue degradation by zinc oxide under different conditions
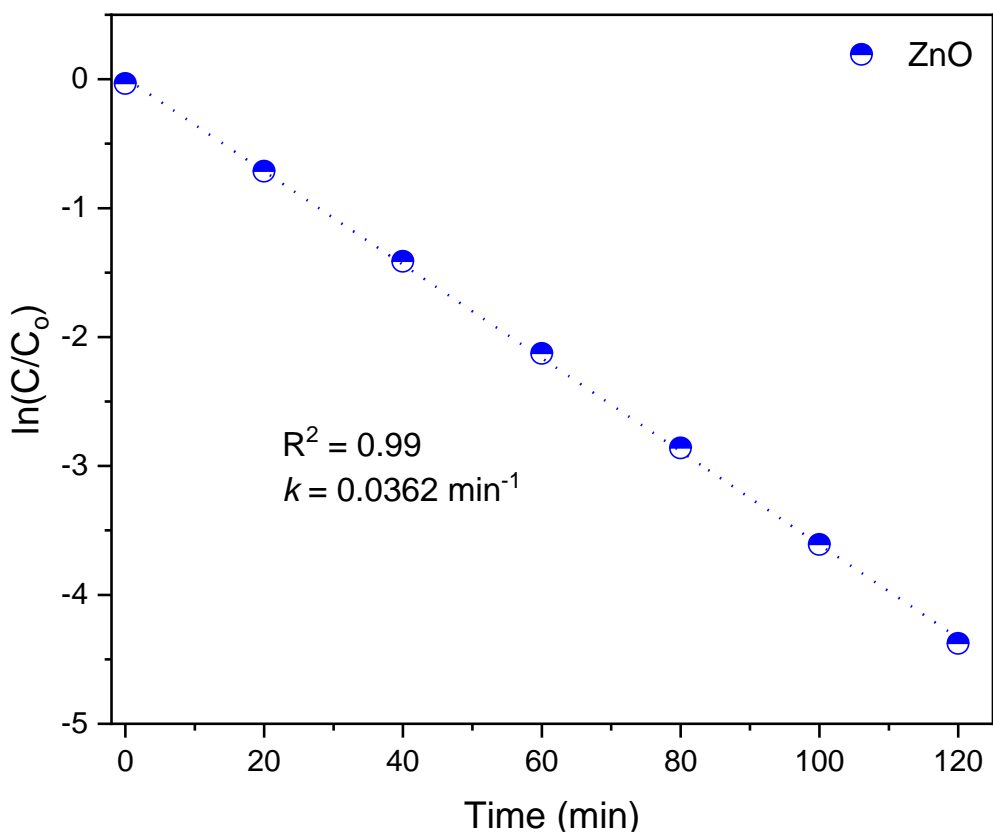
Figure 4.32: Reaction kinetics for degradation of methylene blue by zinc oxide
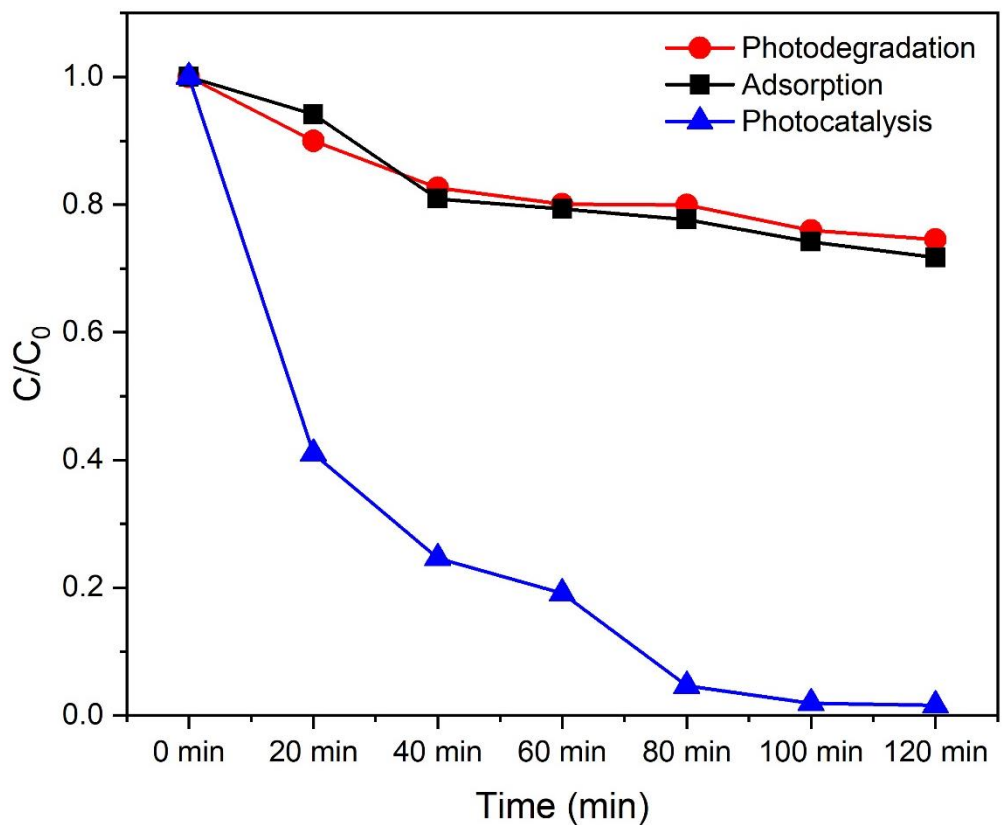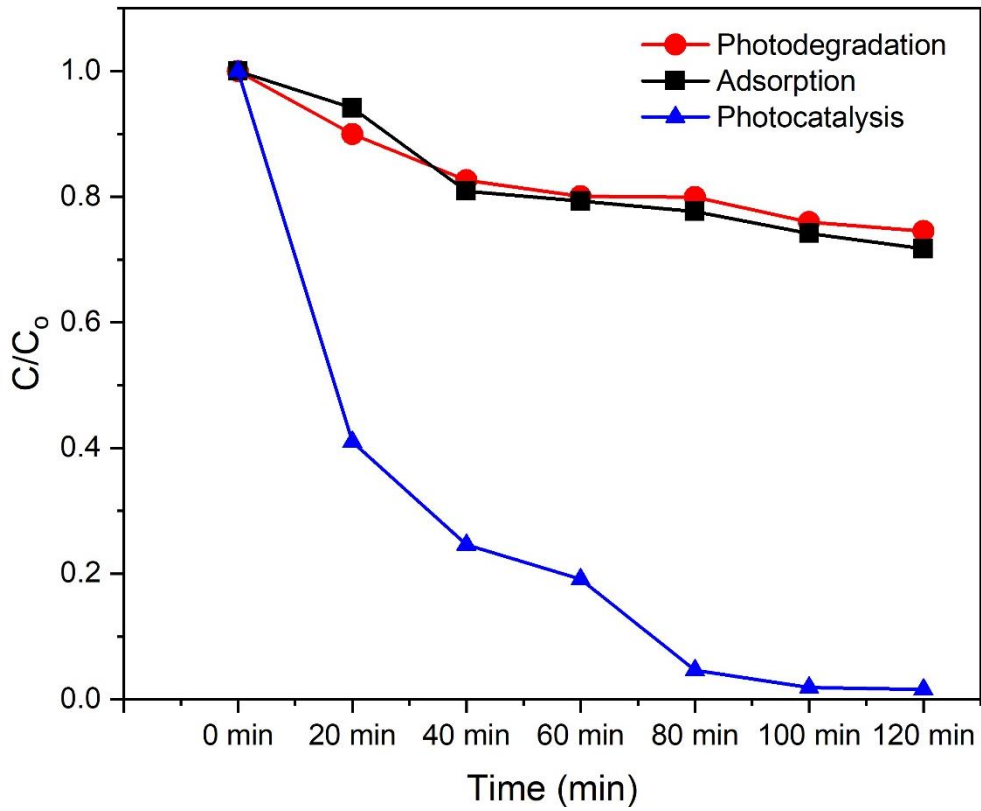
Figure 4.34: Methylene blue degradation by zinc ferrite under different conditions
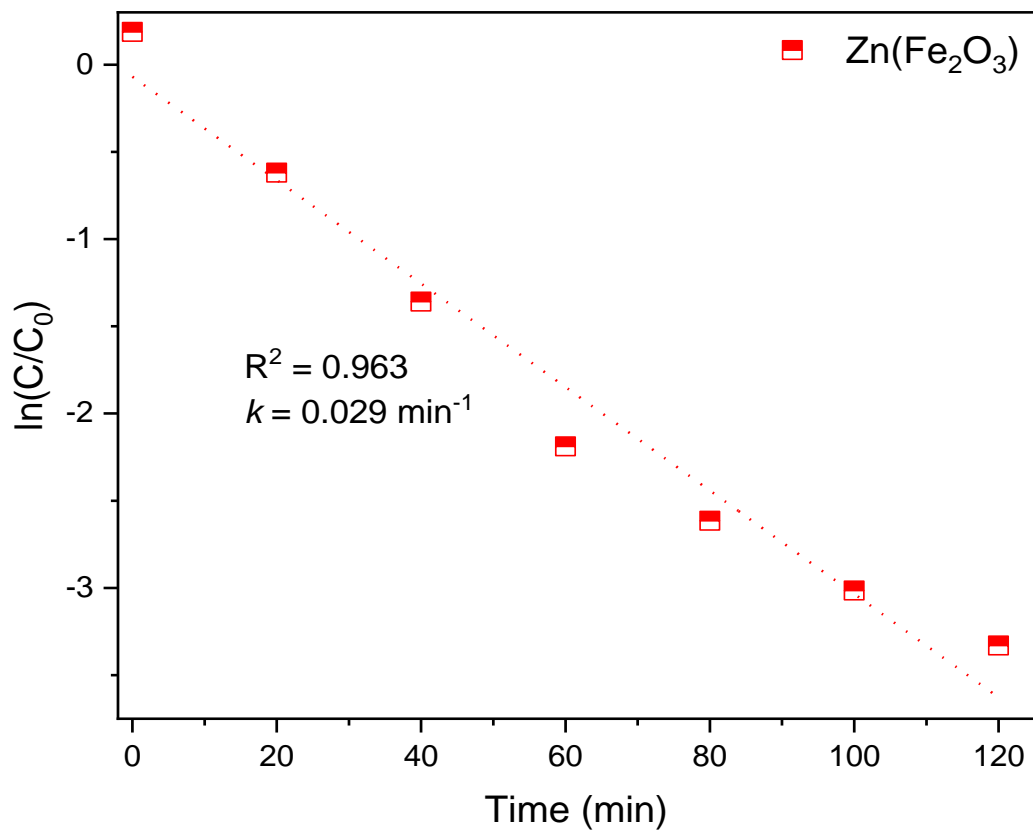
Figure 4.33: Reaction kinetics for methylene blue degradation by zinc ferrite
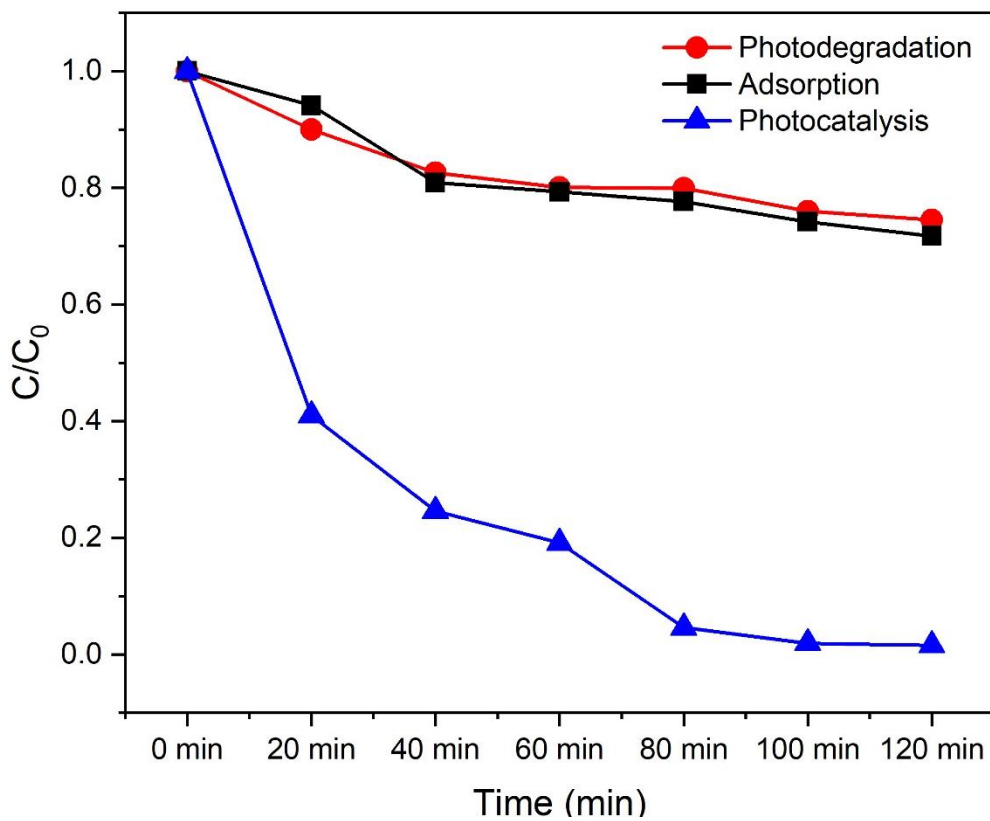
Figure 4.36: Methylene blue degradation by zinc oxide-zinc ferrite composite under different conditions
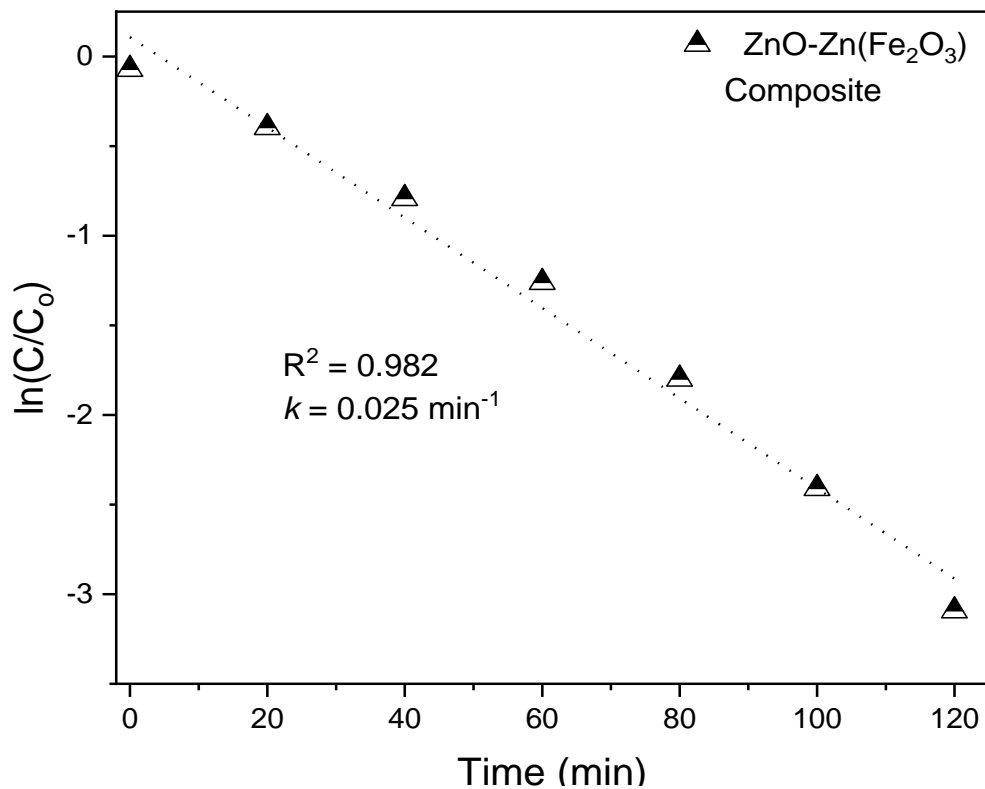
Figure 4.35: Reaction kinetics for methylene blue degradation by zinc oxide-zinc ferrite composite

4.4 Comparative Analysis of Degradation Efficiency

The efficiency of synthesized three materials is compared at wavelength of 665 nm. The following table shows the decrease in concentration over the period of time. It is evident that slight decrease in concentration of MB under light without presence of any catalyst as depicted as photodegradation. While in the presence of catalyst and light, high removal efficiency is observed.

Table 4.7: Table showing decrease in concentration of methylene blue under various conditions

Time	Photodegradation	Photocatalysis (Composite)	Photocatalysis $Zn(Fe_2O_4)$	Photocatalysis (ZnO)
0 min	2.0	2.0	2.0	2.0
20 min	1.7	1.2	1.7	0.8
40 min	1.7	0.9	0.4	0.5
60 min	1.6	0.8	0.2	0.4
80 min	1.6	0.2	0.2	0.1
100 min	1.6	0.2	0.1	0.0
120 min	1.5	0.1	0.1	0.0

The following graphs shows the degradation efficiency over the period of time for ZnO, $Zn(Fe_2O_4)$ and composite material. The samples were characterized in terms of their capacity to eliminate a pollutant; it ideally should be methylene blue or other organic dye but it can be another compound as well. The data is plotted in form of percentage of pollutant degraded at specific intervals of time. The degradation efficiencies obtained are 98.45% for ZnO, 96.45% for $Zn(Fe_2O_4)$, and 95.6 % for the ZnO- $Zn(Fe_2O_4)$ composite. The photocatalytic reaction is carried out at visible light. The amount of visible light that each material absorbs and the ability to form reactive species is proportional to its band gap. The three materials exhibit dissimilar band gaps, and this determines the conversion efficiency of visible lights into electron-hole pairs for the synthesis of ROS in the degradation of pollutants.

Table 4.8: Removal efficiency for all three synthesized materials

Material	Time (min)	Removal Efficiency
Zinc Oxide	120 min	98.45%
Zinc Ferrite	120 min	96.45%
Composite	120 min	95.6%

From the results, it is evident that ZnO showed highest removal efficiency of 98.45%. Though ZnO is proved to show high degradation efficiency under UV light, but its performance in this case under visible light can be associated with its structural modification which makes it more sensitive to visible light, hence overall increasing its efficiency as photocatalyst. $Zn(Fe_2O_4)$ has showed the degradation efficiency of 96.45%, although it is a little lower compared to ZnO, but still it has shown good degradation activity. The use of zinc ferrite is considered efficient for practical applications due to lower band gap energy that enables it to absorb visible light. Lastly, composite showed the degradation efficency of 95.6%. the slight decrease in performnce can be atrributed to the fact that composite material has fewer reaction sites as compared to the individual ZnO and $Zn(Fe_2O_4)$ which allows less interaction with the pollutant. Moreover, better dispersion of ZnO and $Zn(Fe_2O_4)$ may bring about the formation of new phases with lower catalytic activity than the initial materials.
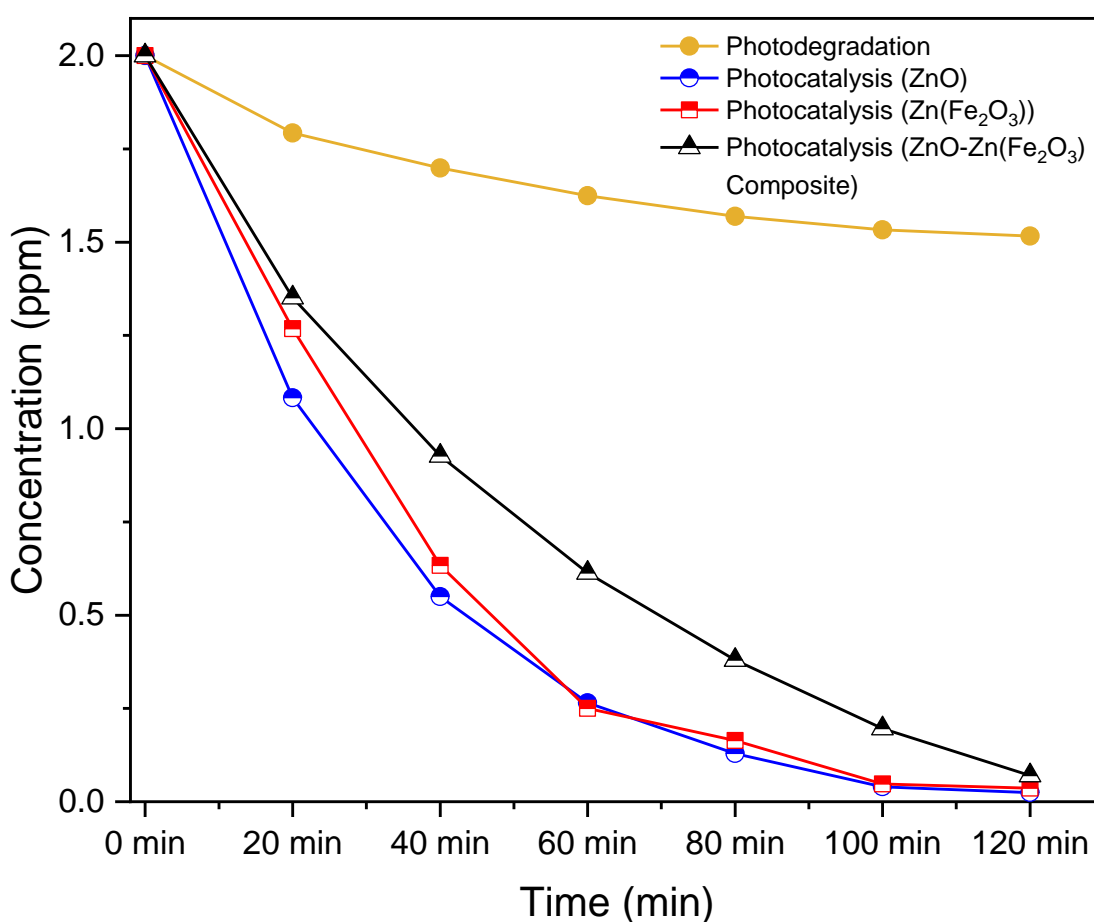
Figure 4.37: Removal of methylene blue under different condition in the presence and absence of catalyst

The following graph shows the kinetic rate constants for MB degradation. k values for the photocatalytic degradation reactions of ZnO, $Zn(Fe_2O_4)$, and the ZnO-$Zn(Fe_2O_4)$ composite are compared. In this case, rate constants are used to quantify the efficiency of the photocatalysts in the degradation of the pollutants within a specific time frame. The graph shows that ZnO has the highest kinetic rate constant of 0.0362 min^{-1} indicating that ZnO degrades the pollutant most quickly out of the three materials. This corroborates the previous results to show that ZnO photodegrades at 98.45% efficiency. Moreover, the k value reveals that ZnO can produce more reactive species within a short time as required in the photocatalytic activity.

$Zn(Fe_2O_4)$ with a rate constant of 0.029 min^{-1} is relatively slower than ZnO for the degradation of pollutants. This lower rate could be attributable for higher electron hole recombination rates which leads to reduced charges carriers availability for the photocatalytic reaction. The composite has shown 95.6% degradation efficency with a rate constant of 0.024 min^{-1} which explains the lower efficency of composite as compared to the individual materials.
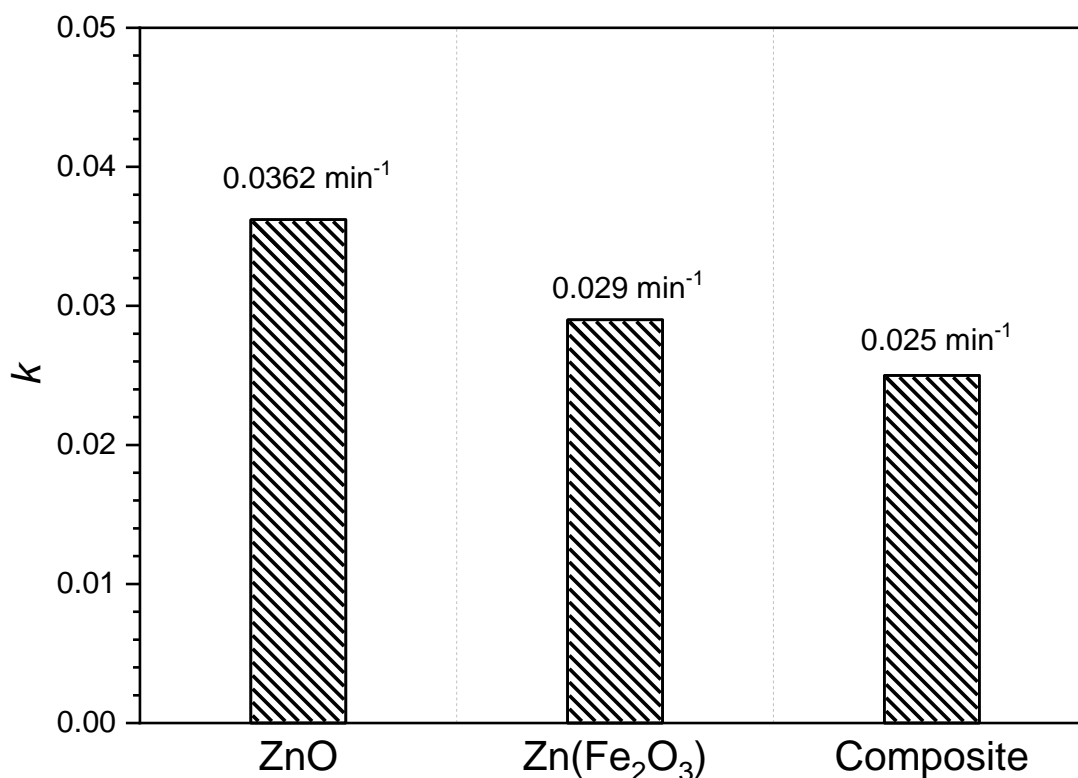
Figure 4.38: Bar graph showing reaction rate constants for three materials

4.5 Post photodegradation Analysis

4.5.1 Post XRD Analysis

For post degradation analysis, XRD was carried out for all 3 materials to observe if there is any phase shift after the reaction. The XRD for all 3 materials showed that no particular phase shift was observed which shows the stability of materials after the reaction. Hence, catalysts can be reused and there is no change in material characteristics.
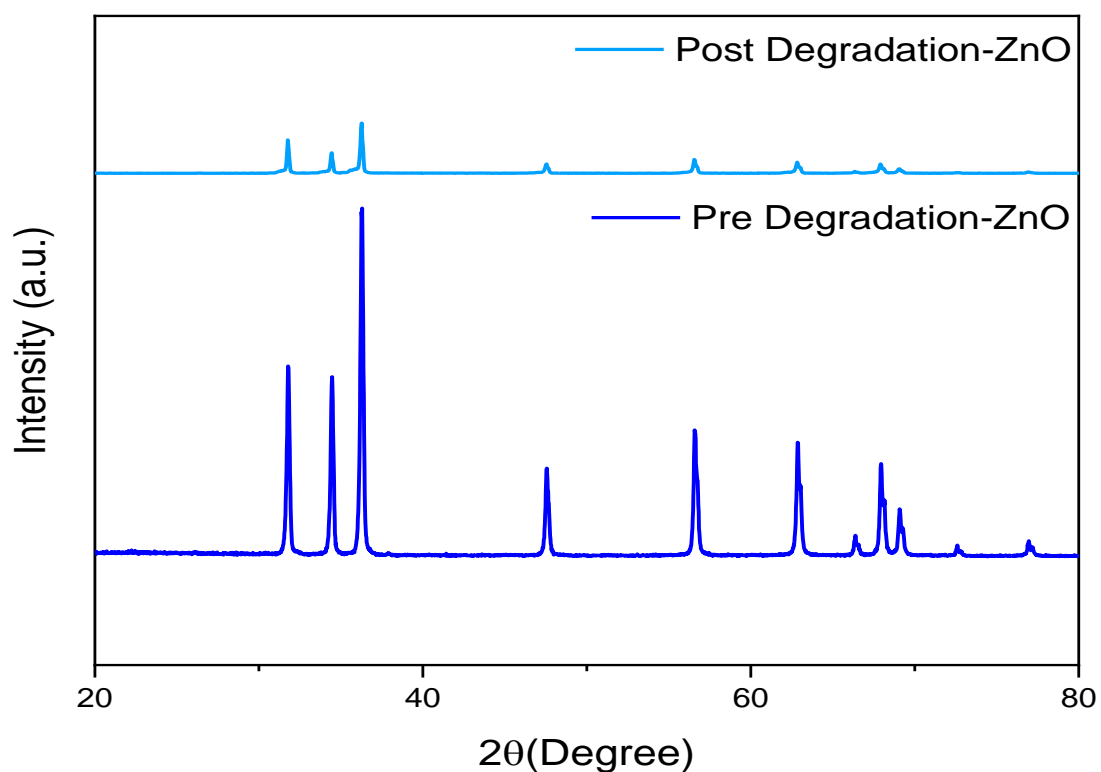
Figure 4.39: Graph showing XRD comparison before and after photocatalytic degradation for zinc oxide
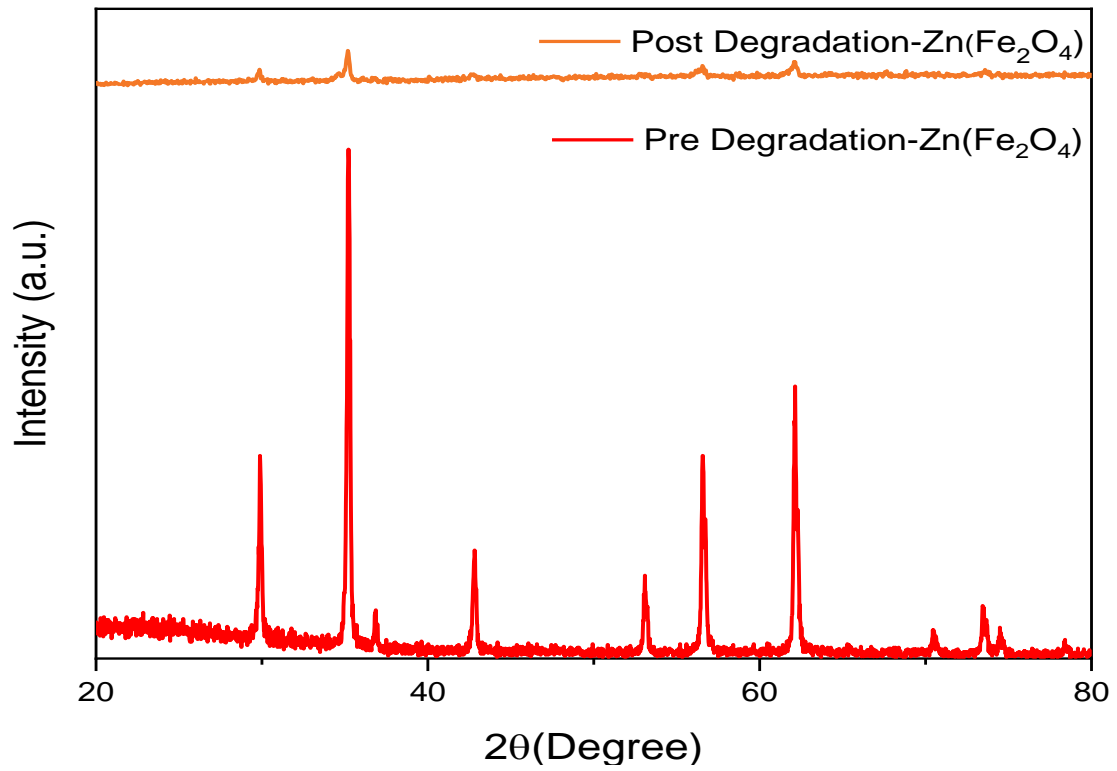
Figure 4.41: Graph showing XRD comparison before and after photocatalytic degradation for zinc ferrite
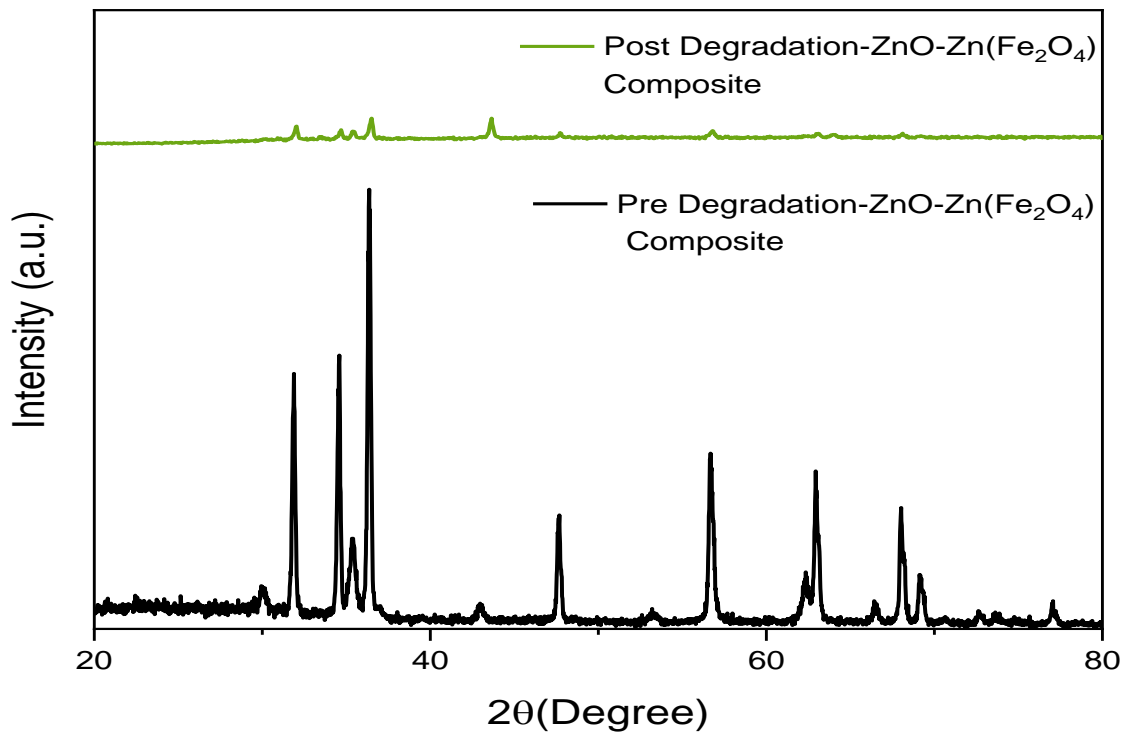
Figure 4.40: Graph showing XRD comparison before and after photocatalytic degradation for composite

4.5.2   Phytotoxicity Analysis

The table below shows the parameters analyzed after 2 weeks. The results showed that degraded water showed a good performance while maintaining the germination rate at optimum level. This shows that treated water from the synthesized catalyst can be successfully used for agricultural purposes without having any toxic effects on plants or hindering their growth. Photocatalytic process effectively minimize the toxic effects on plant growth.

Table 4.9: Comparison of difference in parameters after feeding polluted and treated water to mung beans

Parameter	Water (Control)	Untreated water	Treated Water
Germination %	7	3	5
Shoot length	24.5	15	16
Root length	3.2	2	2.5
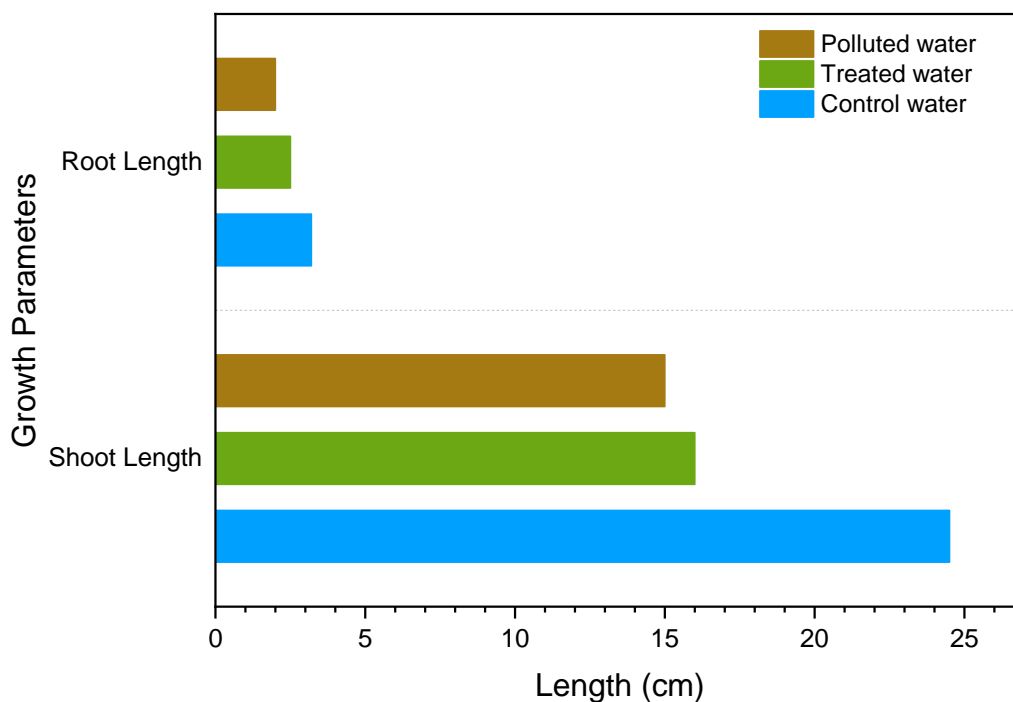
Figure 4.42: Bar graph showing difference in root and shoot length of plants

73

4.5.3 Mineralization Analysis

For mineralization analysis, TOC was performed. TOC analysis is used to analyze the byproducts formed. TOC removal is a key indicator of how effectively the organic pollutants are mineralized into CO_2 and H_2O.

In the graph below, the composite material shows the highest TOC removal, indicating the most complete degradation process, despite its lower photocatalytic efficiency compared to ZnO. This suggests that while ZnO degrades the dye more quickly, the composite might achieve more thorough mineralization of organic contaminants. The TOC percentage removal was calculated as below:

$$\text{TOC removal (\%)} = \frac{\text{TOC}_i - \text{TOC}_t}{\text{TOC}_i} \times 100$$

where TOC_i is theoretical TOC before degradation and TOC_t is analytical TOC after degradation of MB solution.
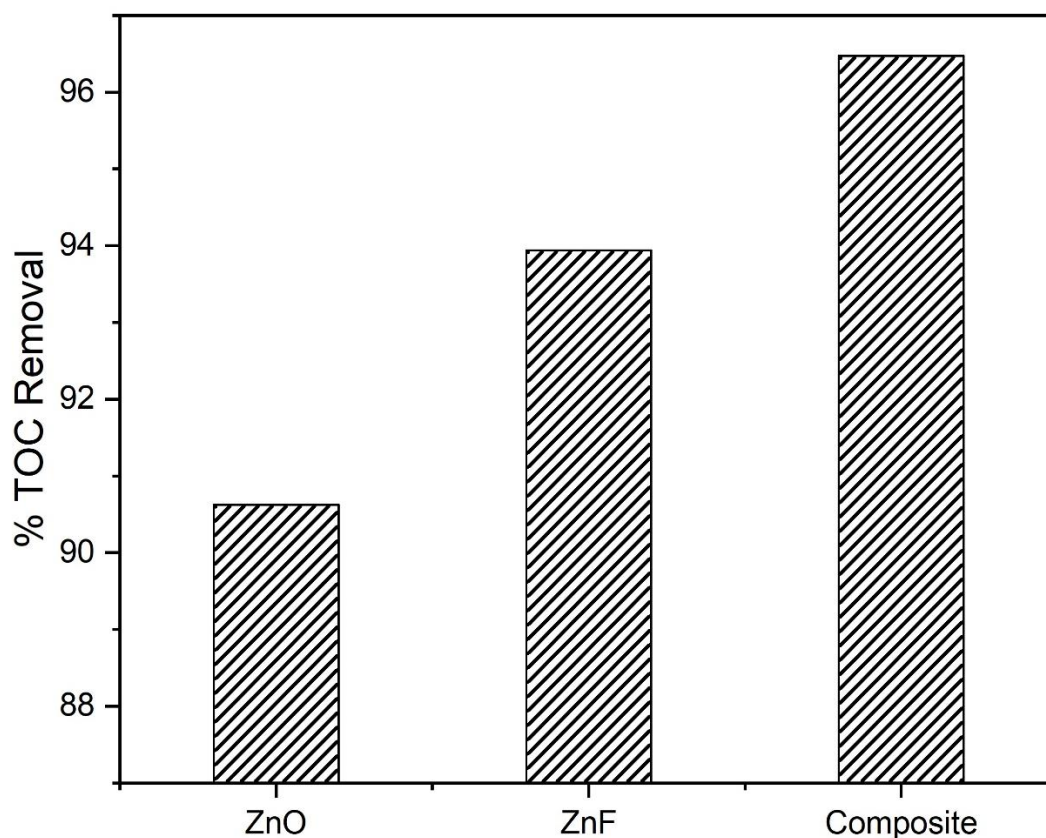
Figure 4.43: Percentage TOC removal by three materials

4.5.4 Cost Analysis

The following tables compares the synthesized three photocatalyst for their cost per 100 g and percentage removal achieved for dye degradation. Although zinc oxide showed highest removal efficiency and is well known for its photocatalytic property and seems to be more cost effective but it cannot be recycled after degradation process due to lack of magnetic property. Zinc ferrite showed good performance and is also due to its magnetic characteristics but it is expensive as compared to the other two photocatalyst. However, the composite material with a blend of zinc oxide and zinc ferrite in a ratio of 1:1, gives a compelling balance between cost and efficiency while providing practical advantages of recyclability due to ferrite present in it. The slight trade off in efficiency can be compensated in broader range of applications due to its magnetic properties. The VSM results confirms the super paramagnetic behavior of composite material. This magnetic property will allow the recyclability of photocatalyst which will reduce the overall cost over time. The recovery of composite material due to its magnetic property can result in cost savings in long run.

Table 4.10: Table showing cost/100g and degradation efficiency of three photocatalyst

Material	Amount (USD)/100 g*	% Efficiency
Zinc oxide	$74/100 g	98%
Zinc ferrite	$90/100g	96%
Composite (1:1)	$82/100g	95%

5 CONCLUSIONS AND RECOMMENDATIONS

This chapter briefly describes about the comprehensive conclusion about the findings obtained from the experimental work focused on synthesis and application for degradation of methylene blue. This chapter will also discuss the contribution of this research in existing knowledge areas, highlights limitations which will pave a way for future recommendations.

5.1 Conclusion

The study proved that the synthesized ZnO, Zn(Fe$_2$O$_4$) and ZnO-Zn(Fe$_2$O$_4$) photocatalyst showed good photocatalytic activity in the degradation of methylene blue under visible light. The material synthesis was successfully carried out using various characterization techniques of XRD, FTIR, RAMAN, SEM, EDX, BET and VSM. These characterizations helped in describing the properties of synthesized materials. Out of all these materials, ZnO has shown to have the highest degradation efficiency of 98.45% followed by Zn(Fe$_2$O$_4$) degrading 96.45% of the dye and the ZnO- Zn(Fe$_2$O$_4$) composite degrading 95.6%. ZnO has been reported to possess higher energy efficiency as compared to Zn(Fe$_2$O$_4$) due to efficient light absorption and reduced electron-hole recombination time. However, the composite material has slightly lower degradation rate, it can be due to charge recombination occur in composites has been claimed by other researchers as well. This is well explained in the kinetic analysis of the data where rate constants were determined to be k = 0.0362 min^{-1} ZnO, k = 0.029 min^{-1} Zn(Fe$_2$O$_4$) and k = 0.025 min^{-1} for the composite. These results conform with the performance shown by each material for degradation of MB. Although the degradation rate was slower in the case of the composite material, its photocatalytic activity is higher than that of many other conventional photocatalysts, which shows a prospect for application.

5.2 Significance

The present work could significantly advance the photocatalysis science in the specific field of wastewater treatment. The results provide information on the photocatalytic activity of ZnO and its composites with Zn ferrite and reflect the efficiency of using such materials under visible light, which is explored less in the photocatalytic processes. The current study is different from most earlier works that have concentrated on UV light as the primary light to induce photocatalytic processes, while this research employs visible light to induce photocatalytic reactions.

Furthermore, the synthesis of the ZnO- Zn(Fe$_2$O$_4$) composite can shed light on the study of the materials synthesized by adopting other composite materials that can exhibit improved mineralization and stability. The doping of ferrite with metal oxide also allows to regenerate and re use photocatalyst in the system.

5.3   Limitations

It is important to understand that the photocatalytic degradation experiments are mostly carried out in the controlled laboratory setting therefore may not provide accurate mimic of real world application. Some factors like water pH, presence of several pollutants and different light intensity was not considered in this study; hence the efficiency of the degradation process may be different. There is a need to fine-tune the synthesis process for the composite material to reduce charge recombination as well as improve its efficiency a notch higher. Moreover, the experiments included only methylene blue as the model pollutant. Future research could be done on other dyes or other organic pollutants because their responses to photocatalytic degradation might be different.

5.4   Recommendations

This section presents suggestions for further study and real-world implementation arising from knowledge discovered in this research. The highlighted recommendations are aimed at the development of scientific knowledge on photocatalytic materials as well as the investigation of discrete aspects of the industrial application of photocatalytic materials.

Further investigation should be made to ensure the synthesis process of the ZnO-Zn(Fe$_2$O$_4$) composite achieves photocatalytic performance under visible light effectively and also show the permanent stability of the ZnO-Zn(Fe$_2$O$_4$) composite. From an industrial point of view, the materials that have been synthesized in this study have enormous application in the environmental sector and particularly in wastewater treatment. High degradation efficiencies observed for both ZnO and Zn(Fe$_2$O$_4$) show their applicability for elimination of organic compounds from water supply systems.

Textile industries which produce high concentration of wastewaters containing dyes will benefit from the use of these materials. It will allow to scale up the photocatalytic activity of ZnO and its improvement in the context of removing industrial effluents since it has few or no ill-effects on the environment and proves to

be cheaper. Multiple stage photocatalytic systems can also be employed in industries in which ZnO-based photocatalysts can be combined with the conventional treatment employing filtering or adsorption techniques. This would turn the system into multi-stage and therefore improve the overall efficiency for removal of pollutants.

Thus, the present work is useful to investigate the photocatalytic degradation of methylene blue using ZnO, $Zn(Fe_2O_4)$ composite. The composite material offers an optimum solution while balancing cost, efficiency, and sustainability. Although zinc oxide and zinc ferrite have their own unique properties, the composite materials offers all of them. Its cost effectiveness, along with removal efficiency and recyclability makes it a good photocatalyst material for dye degradation in water. This material provides versatile properties which makes it applicable and useful in many other industries.

REFERENCES

1. Al-Buriahi, A. K., Al-Gheethi, A. A., Senthil Kumar, P., Radin Mohamed, R. M. S., Yusof, H., Alshalif, A. F., & Khalifa, N. A. (2022). Elimination of rhodamine B from textile wastewater using nanoparticle photocatalysts: A review for sustainable approaches. *Chemosphere*, *287*, 132162.

2. Amin, M. T., Alazba, A. A., & Manzoor, U. (2014). A review of removal of pollutants from water/wastewater using different types of nanomaterials. *Advances in Materials Science and Engineering*, *2014*.

3. Arimi, A., Megatif, L., Granone, 2018, undefined. (n.d.). Visible-light photocatalytic activity of zinc ferrites. *Elsevier*.

4. Basavanagoudra, H., Tanakanti, R., Patil, M. K., Inamdar, S. R., & Goudar, K. M. (2021). Synthesis, Characterization, and Properties of Spinel Zinc Ferrite Nanoparticles by Chemical Coprecipitation Technique. *Macromolecular Symposia*, *400*(1), 2100138.

5. Cai, Z., Sun, Y., Liu, W., Pan, F., Sun, P., and, J. F.-E. S., & 2017, undefined. (n.d.). An overview of nanomaterials applied for removing dyes from wastewater. *Springer*.

6. Cellulose, F. U.-, & 2021, undefined. (n.d.). Environmental hazard in textile dyeing wastewater from local textile industry. *Springer*

7. Charradi, K., Ahmed, Z., BenMoussa, M. A., Beji, Z., Brahmia, A., Othman, I., Haija, M. A., Chtourou, R., & Keshk, S. M. A. S. (2022). A facile approach for the synthesis of spinel zinc ferrite/cellulose as an effective photocatalyst for the degradation of methylene blue in aqueous solution. *Cellulose*, *29*(4), 2565–2576.

8. Davis, K., Yarbrough, R., Froeschle, M., White, J., & Rathnayake, H. (2019). Band gap engineered zinc oxide nanostructures via a sol–gel synthesis of solvent driven shape-controlled crystal growth.

9. Demirci, Y., Pekel, L., electrochemical, M. A.-I. journal of, & 2015, undefined. (n.d.). Investigation of different electrode connections in electrocoagulation of textile wastewater treatment. *Elsevier*.

10. Elshypany, R., Selim, H., Zakaria, K., Moustafa, A. H., ASadeek, S., Sharaa, S., Raynaud, P., Nada, A. A., Elab, al, elshypany, R., & Sadeek, S. A. (2021).

11. Fakhari, S., Jamzad, M., & Kabiri Fard, H. (2019). Green synthesis of zinc oxide nanoparticles: a comparison. *Green Chemistry Letters and Reviews*, *12*(1), 19–24.

12. Gegova-Dzhurkova, R., Nesheva, D., Molecules, I. S.-, & 2024, undefined. (n.d.). Enhanced Photocatalytic Performance under Ultraviolet and Visible Light Illumination of ZnO Thin Films Prepared by Modified Sol-Gel Method.

13. Giram, D., (IJCT), A. D.-I. J. of C. T., & 2024, undefined. (n.d.). Synthesis and characterization of Fe doped ZnO nanoparticles for the photocatalytic degradation of Eriochrome Black-T dye.

14. Gupta, S., Chang, C., Lai, C., Engineering, N. T.-C. P. B., & 2019, undefined. (n.d.). Hybrid composite mats composed of amorphous carbon, zinc oxide nanorods and nickel zinc ferrite for tunable electromagnetic interference shielding. *Elsevier*.

15. Hammouche, J., Gaidi, M., Columbus, S., & Omari, M. (2021). Enhanced Photocatalytic Performance of Zinc Ferrite Nanocomposites for Degrading Methylene Blue: Effect of Nickel Doping Concentration. *Journal of Inorganic and Organometallic Polymers and Materials*, *31*(8), 3496–3504.

16. Hedayati, K., Tamiji, M., Research, D. G.-J. of S. E., & 2020, undefined. (n.d.). Photo-catalyst zinc ferrite-zinc oxide nanocomposites applicable for water purification under solar irradiation. *Sid.Ir*.

17. Holkar, C. R., Jadhav, A. J., Pinjari, D. V, Mahamuni, N. M., & Pandit, A. B. (2016). A critical review on textile wastewater treatments: possible approaches. *Journal of Environmental Management*, *182*, 351–366.

18. Karthik, V., Saravanan, K., … N. S.-E. E., & 2016, undefined. (n.d.). Bioremediation of dye bearing effluents using microbial biomass. *Academia.Edu*.

19. Kumar, J., Bolimera, U., Proceedings, P. T.-A. C., & 2019, undefined. (n.d.). Direct sunlight responsive ZnO photocatalyst: Highly efficient photodegradation of Methylene Blue. *Pubs.Aip.Org*.

20. Kumari, H., Suman, S. ·, Ranga, R., Chahal, S., Seema, ·, Sourabh, D. ·, Sandeep Kumar, S. ·, Kumar, P., Suresh Kumar, ·, Kumar, A., & Parmar, R. (2023). A review on photocatalysis used for wastewater treatment: dye degradation. *Springer*, *234*(6), 349.

21. Liu, H., Li, A., Ding, X., Yang, F., & Sun, K. (2019). Magnetic induction heating properties of Mg1-xZnxFe2O4 ferrites synthesized by co-precipitation method. *Solid State Sciences*, *93*, 101–108.

22. Manzoor, J., and, M. S.-I. of textile dyes on public health, & 2020, undefined. (2020). Impact of textile dyes on human health and environment.

23. Meehan, K., Jurjevich, J. R., Chun, N. M. J. W., & Sherrill, J. (2020). Geographies of insecure water access and the housing–water nexus in US cities.

24. Meky, A., Hassaan, M., Fetouh, H., Reports, A. I.-S., & 2023, undefined. (n.d.-a). Cube-shaped Cobalt-doped zinc oxide nanoparticles with increased visible-light-driven photocatalytic activity achieved by green co-precipitation synthesis. *Nature.Com*.

25. Meky, A., Hassaan, M., Fetouh, H., Reports, A. I.-S., & 2023, undefined. (n.d.-b). Cube-shaped Cobalt-doped zinc oxide nanoparticles with increased visible-light-driven photocatalytic activity achieved by green co-precipitation synthesis. *Nature.Com*.

26. Musa, M., Sustainability, S. I.-, & 2021, undefined. (2021). Physical and biological treatment technologies of slaughterhouse wastewater.

27. Mushtaq, K., Saeed, M., Gul, W., Munir, M., Firdous, A., Yousaf, T., Khan, K. B., Sarwar, H. M. R., Riaz, M. A., & Zahid, S. (2020). Synthesis and characterization of TiO2 via sol-gel method for efficient photocatalytic degradation of antibiotic ofloxacin. *Inorganic and Nano-Metal Chemistry*, *50*(7), 580–586.

28. Neoh, C. H., Noor, Z. Z., Mutamim, N. S. A., & Lim, C. K. (2016). Green technology in wastewater treatment technologies: Integration of membrane bioreactor with various wastewater treatment systems. *Chemical Engineering Journal*, *283*, 582–594.

29. Noman, E., Al-Gheethi, A., Talip, B. A., Mohamed, R., & Kassim, A. H. (2021). Decolourization of Dye Wastewater by A Malaysian isolate of Aspergillus iizukae 605EAN Strain: A Biokinetic, Mechanism and Microstructure Study. *International Journal of Environmental Analytical Chemistry*, *101*(11), 1592–1615.

30. Pereira, L., & Alves, M. (2012). Dyes—Environmental Impact and Remediation. *Environmental Protection Strategies for Sustainable Development*, 111–162.

31. Pratap, B., Kumar, S., Nand, S., Azad, I., Bharagava, R. N., Romanholo Ferreira, L. F., & Dutta, V. (2023). Wastewater generation and treatment by various eco-friendly technologies: Possible health hazards and further reuse for environmental safety. *Chemosphere*, *313*, 137547.

32. Pratap, B., Kumar, S., Purchase, D., Bharagava, R. N., & Dutta, V. (2023). Practice of wastewater irrigation and its impacts on human health and environment: a state of the art. *International Journal of Environmental Science and Technology*, *20*(2), 2181–2196.

33. Santhosh, C., Velmurugan, V., Jacob, G., S. J.-C. E., & 2016, undefined. (n.d.). Role of nanomaterials in water treatment applications: a review. *Elsevier*.

34. Saravanan, A., Deivayanai, V., Chemosphere, P. K.-, & 2022, undefined. (n.d.). A detailed review on advanced oxidation process in treatment of wastewater: Mechanism, challenges and future outlook. *Elsevier*.

35. Shandilya, P., Sambyal, S.R. S.-F., & 2021, undefined. (n.d.). Recent advancement on ferrite based heterojunction for photocatalytic degradation of organic pollutants: a review.

36. Sharma, N., Singh, A., & Batra, N. (2019). *Modern and Emerging Methods of Wastewater Treatment*. 223–247.

37. Silambarasu, A., Manikandan, A., & Balakrishnan, K. (2017). Room-Temperature Superparamagnetism and Enhanced Photocatalytic Activity of Magnetically Reusable Spinel $Zn(Fe_2O_4)$ Nanocatalysts. *Journal of Superconductivity and Novel Magnetism*, *30*(9), 2631–2640.

38. Singh, P., Mohan, B., Madaan, V., Ranga, R., Kumari, P., Kumar, S., Bhankar, V., Kumar, P., & Kumar, K. (2022). Nanomaterials photocatalytic activities for waste water treatment: a review.

39. Sun, J., Dong, S., Feng, J., Yin, X., Molecular, X. Z.-J. of, & 2011, undefined. (n.d.). Enhanced sunlight photocatalytic performance of Sn-doped ZnO for Methylene Blue degradation. *Elsevier*.

40. Sun, W., Meng, S., Zhang, S., Zheng, X., Ye, X., Fu, X., & Chen, S. (2018). Insight into the Transfer Mechanisms of Photogenerated Carriers for Heterojunction Photocatalysts with the Analogous Positions of Valence Band and Conduction Band: A Case Study of ZnO/TiO_2. *Journal of Physical Chemistry C*, *122*(27), 15409–15420.

41. Tamiji, M., Hedayati, K., & Ghanbari, D. (2020). Photo-catalyst zinc ferrite-zinc oxide nanocomposites applicable for water purification under solar irradiation. *Journal of Solar Energy Research*, *5*(4), 568–579.

42. Teuntje, E., & Kakes, M. (2020). The Protection of the Human Right to Safe Drinking Water in the Context of Climate Change: Considering Lessons from the Water Crisis in the City of Cape.

43. Villaseñor-Basulto, D., Bandala, E., I. R.-S., & 2022, undefined. (n.d.). Synthesis and photocatalytic applications of CuxO/ZnO in environmental remediation. *Elsevier*.

44. Westall, F., & Brack, A. (2018). The Importance of Water for Life. *Space Science Reviews*, *214*(2).

45. Yashni, G., Al-Gheethi, A., Mohamed, R., Chemosphere, N. D.-V.-, & 2021, undefined. (n.d.). Bio-inspired ZnO NPs synthesized from Citrus sinensis peels extract for Congo red removal from textile wastewater via photocatalysis: Optimization, mechanisms. *Elsevier*.

46. Zhang, Y., Shaad, K., Vollmer, D., Water, C. M.-, & 2021, undefined. (n.d.). Treatment of textile wastewater using advanced oxidation processes—a critical review. *Mdpi.Com*.